Materials Today Bio 7 (2020) 100071

Contents lists available at ScienceDirect

Materials Today Bio

journal homepage: www.journals.elsevier.com/materials-today-bio

Engineering osteogenic microenvironments by combination of multilayers from collagen type I and chondroitin sulfate with novel cationic liposomes

Y.A. Brito Barrera [a], G. Hause [b], M. Menzel [c], C.E.H. Schmelzer [c], E. Lehner [d], K. Mäder [d], C. Wölk [e], T. Groth [a,f,*]

[a] Department Biomedical Materials, Institute of Pharmacy, Martin Luther University Halle–Wittenberg, Heinrich Damerow Strasse 4, 06120, Halle (Saale), Germany
[b] Martin Luther University Halle-Wittenberg, Biocenter, Weinbergweg 22, 06120, Halle (Saale), Germany
[c] Department of Biological and Macromolecular Materials, Fraunhofer Institute for Microstructure of Materials and Systems (IMWS), Walter-Hülse-Strasse 1, 06120, Halle (Saale), Germany
[d] Department Pharmaceutical Technology, Institute of Pharmacy, Martin Luther University Halle–Wittenberg, Kurt-Mothes Straße 3, 06120, Halle (Saale), Germany
[e] Pharmaceutical Technology, Institute of Pharmacy, Faculty of Medicine, Leipzig University, 04317, Leipzig, Germany
[f] Interdisciplinary Center of Materials Science, Martin Luther University Halle-Wittenberg, D-06099, Halle (Saale), Germany

ARTICLE INFO

Keywords:
C2C12 myoblasts
cationic lipids
chondroitin sulfate
collagen I
internalization
osteogenic differentiation
polyelectrolyte multilayer system

ABSTRACT

Cationic liposomes composed of a novel lipid (N-{6-amino-1-[N-(9Z) -octadec9-enylamino] -1-oxohexan-(2S) -2-yl} –N'- {2- [N, N-bis(2-aminoethyl) amino] ethyl} -2-hexadecylpropandiamide) (OO4) and dioleoylphosphatidylethanolamine (DOPE) possess high amounts of amino groups and are promising systems for lipofection. Moreover, these cationic liposomes can also be used as a polycationic entity in multilayer formation using layer-by-layer technique (LbL), which is a method to fabricate surface coatings by alternating adsorption of polyanions and polycations. Since liposomes are suitable for endocytosis by or fusion with cells, controlled release of their cargo on site is possible. Here, a polyelectrolyte multilayer (PEM) system was designed of chondroitin sulfate (CS) and collagen type I (Col I) by LbL technique with OO4/DOPE liposomes embedded in the terminal layers to create an osteogenic microenvironment. Both, the composition of PEM and cargo of the liposomes were used to promote osteogenic differentiation of C2C12 myoblasts as in vitro model. The internalization of cargo-loaded liposomes from the PEM into C2C12 cells was studied using lipophilic (Rhodamine-DOPE conjugate) and hydrophilic (Texas Red–labeled dextran) model compounds. Besides, the use of Col I and CS should mimic the extracellular matrix of bone for future applications such as bone replacement therapies. Physicochemical studies of PEM were done to characterize the layer growth, thickness, and topography. The adhesion of myoblast cells was also evaluated whereby the benefit of a cover layer of CS and finally Col I above the liposome layer was demonstrated. As proof of concept, OO4/DOPE liposomes were loaded with dexamethasone, a compound that can induce osteogenic differentiation. A successful induction of osteogenic differentiation of C2C12 cells with the novel designed liposome-loaded PEM system was shown. These findings indicate that designed OH4/DOPE loaded PEMs have a high potential to be used as drug delivery or transfection system for implant coating in the field of bone regeneration and other applications.

Abbreviations: AFM, Atomic force microscopy; CLSM, Confocal Laser Scanning Microscopy; Col I, Collagen I; CS, chondroitin sulfate; Dex, Dexamethasone; DLS, Dynamic light scattering; DMEM, Dulbecco's modified Eagle's medium; DOPE, dioleoylphosphatidylethanolamine; ECM, Extracellular matrix; GAG, Glycosaminoglycan; LbL, Layer-by-Layer technique; OO4, (N-{6-amino-1-[N-(9Z) -octadec9-enylamino] -1-oxohexan-(2S) -2-yl} -N'- {2- [N, N-bis(2-aminoethyl) amino] ethyl} -2-hexadecylpropandiamide); PEI, Polyethylenimine; PEM, Polyelectrolyte multilayer; PBS, Phosphate-buffered saline; SEM, Scanning electron microscopy; SPR, Surface plasmon resonance; TEM, Transmission electron microscopy; WCA, Water contact angle.

* Corresponding author. Department Biomedical Materials, Institute of Pharmacy, Martin Luther University Halle–Wittenberg, Heinrich Damerow Strasse 4, 06120, Halle (Saale), Germany.

E-mail address: thomas.groth@pharmazie.uni-halle.de (T. Groth).

https://doi.org/10.1016/j.mtbio.2020.100071
Received 22 April 2020; Received in revised form 15 July 2020; Accepted 16 July 2020
Available online 31 July 2020

1. Introduction

Major problems that implants may cause have been related to poor healing related to recognition as foreign body with reduction or loss of function after device implantation [1]. These and other complications during the application of medical implants have fostered significant efforts in surface modification of biomaterials to achieve a well-defined and controlled interface between the material and host tissues [2]. Various studies have been focused on modifying the surfaces by physical and chemical means to improve biocompatibility and control cell behavior by establishing desired physicochemical properties, such as surface charge [3], wettability [4], topography [5], stiffness [6], and the presence of specific chemical groups on the surface [7].

Surface properties of scaffold materials are also critical in tissue engineering due to the adhesion and spreading controls functioning of cells including gene expression, proliferation, and differentiation [8,9]. However, tissue engineering goes beyond conventional biomedical implant technology because of degradable materials that are combined with cells and bioactive molecules to mimic the natural process of tissue regeneration [10,11]. Besides synthetic polymers such as polylactic acid, biopolymers such as polysaccharides (e.g. chitosan, hyaluronan, etc.) and proteins (e.g. collagens, gelatin, silk) have been used for making hydrogels, porous scaffolds, and coatings due to their biocompatibility, bioactivity, degradability, and often abundance [12]. Bioactivity of collagens and other proteins of the extracellular matrix (ECM) is due to their interaction with cell adhesion molecules, such as integrins followed by signal transduction processes [13]. On the other hand, polysaccharides in particular glycosaminoglycan's (GAG) as class of animal glycans can address directly cellular receptors followed by signal transduction like hyaluronan-CD 44 ligation [14] or interact with matrix proteins and growth factors that lead to stabilization of growth factors and facilitate their binding to the corresponding cellular receptors as known for heparan sulfate with bone morphogenic proteins (BMPs) and corresponding BMP receptors [15]. Hence, ECM proteins like collagens from animal sources are used to make protein coatings on implants to guide cell attachment [16]. Moreover, combinations of GAGs with proteins like collagen I can be used for the formation of bioactive coatings, such as multilayers fabricated through layer-by-layer technique (LbL) [17].

The LbL technique is a method to fabricate coatings by alternating adsorption of polyanions and polycations, occurring via electrostatic or non-electrostatic interaction and is considered as a promising technique to modify material surfaces [18]. The LbL assembly can be realized by different methods such as dip-coating, spin-coating, and perfusion [18]. Since many biomolecules such as proteins and GAG represent polyelectrolytes, LbL can be used for biomedical applications due to inclusion of bioactive molecules [10,19]. Nowadays, biomaterials have been advanced through the design of biocompatible systems for controlled drug release in combination with the development of scaffolds in the area of tissue engineering [20]. The advantage of liposomes is that they can interact with cells through several mechanisms, such as endocytosis, fusion with the cell membrane, lipid exchange, and adsorption [21]. The use of liposomes as building blocks for LbL films has attractive aspects, including the ability to internalize a functional cargo, such as lipophilic or hydrophilic drugs or other bioactive compounds like DNA for transfection and controlled assembly of the liposome within LbL films without hampering the activity of functional molecules in the core or lipid part [22]. First approaches were made using natural phospholipids coated by poly-L-lysine to obtain a cationic surface enabling LbL deposition [23,24]. Nevertheless, the toxicity of poly-L-lysine represents a challenge for biomedical application [25]. An approach with negatively charged liposomes composed of phosphatidylserine or phosphatidylglycerol also allows LbL deposition of liposomes without stabilizing polymers [26]. Apart from the use of natural lipids, the use of novel synthetic lipids may represent an interesting strategy to modify liposomes' features toward better interaction with cells and embedding in LbL multilayer systems.

Malonic acid diamides are a group of peptide-mimicking cationic lipids, which are useful components to formulate liposomes with a positive surface charge, low cytotoxicity, and extremely high transfection efficiency [27,28]. These cationic liposomes can potentially be embedded in multilayer films based on LbL to retain these lipid containers after the localized release of a bioactive compound or alternatively, release the entire container with functional cargos from surfaces into the cells or surrounding tissue [22]. Liposomes have been considered as carrier systems, controlling the delivery of genetic material and other biomolecules, but little is known about their behavior as component of LbL multilayers, yet. Hence, this article investigates the deposition of novel cationic liposomes composed of (N-{6-amino-1-[N-(9Z) -octadec9-enylamino] -1-oxohexan-(2S) -2-yl} –N'- {2- [N, N-bis(2-aminoethyl) amino] ethyl} -2-hexadecylpropandiamide) (OO4) and dioleoylphosphatidylethanolamine (DOPE) [29], a peptide-mimicking cationic amphiphilic of the malonic acid diamide family, onto polyelectrolyte multilayer (PEM) system. Col I and CS were used as polycations and polyanions, respectively, to mimic the ECM of bone as it was done in a previous study promoting osteogenic differentiation of mesenchymal stem cells [17,30]. The work focuses on characterization of multilayer formation process and surface properties of the resulting films

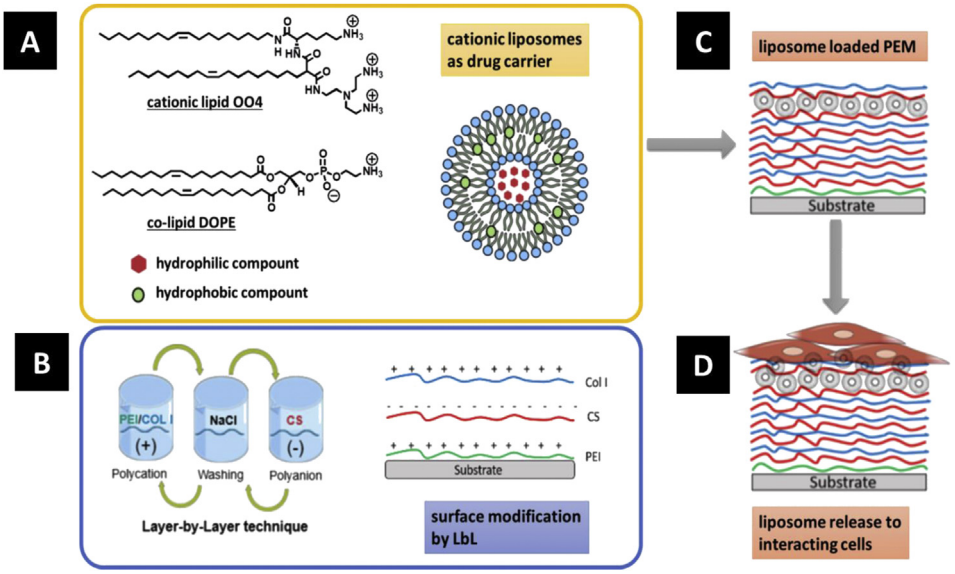

Fig. 1. A) Schematic illustration of the preparation of liposomes using the cationic lipid OO4 and the zwitterionic co-lipid DOPE (protonation state at pH 4) [27]. The liposomes can be used as a carrier for hydrophilic and lipophilic drugs. **B)** Due to the cationic charge [31], the liposomes can be embedded in polyelectrolyte multilayers (PEMs), which are prepared from collagen I and chondroitin sulfate using the layer-by-layer technique. Poly (ethylene imine) was used for the initial modification of the substrate to achieve a positive surface charge. **C/D)** The liposomes embedded in the PEM can be internalized by cells growing on the modified substrate.

including surface zeta potential, roughness, topography, and wettability. Besides studies on adhesion and viability of C2C12 myoblast cells on the films, also cellular uptake of liposomes from PEM loaded with hydrophilic and lipophilic fluorescence-labeled model substances was studied. Finally, a proof-of-concept study with liposomes loaded with dexamethasone to promote osteogenic differentiation of cells was performed. Fig. 1 summarizes the content of this work.

2. Materials and methods

2.1. Preparation of liposomes

Liposomes were prepared by film hydration procedure. The lipids OO4 and DOPE were dissolved in chloroform/methanol (8:2, v/v) in a round bottom flask and mixed to a molar ratio of 1:3 (cationic lipid/phospholipid). The solvent was evaporated for 1 h at 200 mbar. Then, 150 mM of NaCl with 10 mM acetic acid at pH 4 was added to final concentration of 1 mg/mL. Afterward, the lipid dispersion was incubated at 50°C and shaking gently for 30 min at 1,400 rpm (Eppendorf Thermomixer 5436) followed by sonication at 37 kHz and 50°C for 5 min. 1,2-dioleoyl-sn-glycero-3-phosphoethanolamine-N- (lissamine rhodamine B sulfonyl) ammonium salt (Avanti Polar lipids); Rhodamine-DOPE-loaded liposomes were prepared with the same method using a molar ratio of 1:3:0.05 (n_{OO4}:n_{DOPE}:$n_{Rhodamine\text{-}DOPE}$).

2.1.1. Loading of liposomes with dexamethasone

The liposomes were prepared with a concentration of 1 mg/mL total lipid (50 μg/mL dexamethasone) following the liposome preparation protocol explained in 2.2 using chloroform/methanol (8:2, v/v) stock solutions of OO4, DOPE, and dexamethasone combined to a molar ratio of 1:3:0.2 (n_{OO4}:n_{DOPE}:n_{Dex}). For determination of the encapsulation of dexamethasone we varied an ultracentrifugation protocol [32]. Briefly, 0.8 μL of the liposomes were diluted to 9 mL with 10 mM acetic acid buffer at pH 4 containing 150 mM of NaCl. Afterward the liposome dispersion was centrifuged for 4 h with 35,000×*g* using an ultracentrifuge (TL 100, Beckman Coulter GmbH, Krefeld, Deutschland). Afterward, 0.5 mL of the supernatant was freeze-dried and dissolved in 100 μL methanol for high-performance liquid chromatography (HPLC) analysis. A modified method from United States Pharmacopeia was used to quantify the amount of dexamethasone in the supernatant. A Jasco HPLC system with a PU-1580 Pump equipped with LG-1580-04 quaternary gradient unit, AS 1559 Intelligent Auto Sampler, UV 1559 intelligent UV/VIS Detector (all Jasco, Oklahoma City, USA), Purospher® Star RP-18 endcapped (5 μm) column (Merck Millipore, Billerica, Massachusetts, USA), operated at 40 °C, were used. Methanol was used as the mobile phase at a flow of 1 mL/min A 20 μL of sample was injected and analyzed at λ = 258 nm. Data recording and processing were carried out with the software ChromNAV Ver.2 (Jasco, Oklahoma City, USA).

2.1.2. Loading of liposomes with Texas Red–labeled dextran

Liposomes were prepared as stated above (2.2) with the difference that the final concentration was 4 mg/mL and the hydration buffer contained additionally 0.4 mg/mL Texas Red dextran (Texas Red dextran [3,000 Da, lysine fixable] was purchased from Thermo Fisher Scientific). Afterward, the loaded liposomes were purified by size exclusion chromatography using PD-10 Columns (GE Healthcare) and 10 mM acetate buffer pH 4 with 150 mM of NaCl as elution buffer.

2.2. Characterization of liposomes

2.2.1. Dynamic light scattering

The size distribution was characterized by Zetasizer Nano ZS ZEN3600 (Malvern Instruments, Worcestershire, UK). The sample was measured three times; each run consisted 10 runs with a duration of 20 s at 25°C. The viscosity η = 0.8872 mPa·s and the refractive index of 1.33 at 25°C were assumed, as has been described previously [33]. The Zetasizer software 7.12 was used for data evaluation.

2.2.2. Zeta potential measurements

The zeta potential measurements were carried out with the laser Doppler electrophoresis technique using Zetasizer Nano ZS ZEN3600 (Malvern Instruments, Worcestershire, UK). Three measurements were performed of 20 runs with a voltage of 50 V at 25°C. The viscosity η = 0.8872 mPa·s, dielectric constant ε = 78.5 F/m and refractive index of 1.33 were assumed. The diffusion of aggregates was converted into the zeta potential using Smoluchowski equation $\zeta = \mu\,\eta/\varepsilon$ (Zetasizer software 7.12) [33].

2.2.3. Transmission electron microscopy

For freeze-fracture analysis, the samples were firstly fixed with a propane jet freeze device JFD 030 (BAL-TEC, Balzers, Liechtenstein). Afterward, the samples were frozen fractured at −150 °C without etching with a freeze-fracture/freeze etching system BAF 060 (BAL-TEC, Balzers, Liechtenstein). The surfaces on the fractures were shadowed with platinum (2 nm layer, shadowing angle 45 degrees) and subsequently with carbon (20 nm layer, shadowing angle 90degrees). The replicas were floated into a sodium chloride solution (4% available chlorine) for 30 min, rinsed in distilled water for 10 min, washed in 30% acetone for 30 min, and finally rinsed in distilled water for 10 min. Thereafter, the replicas were placed on copper grids coated with a Formvar film for imaging [33].

Vitrified specimens for CryoTEM were prepared using a blotting procedure, performed in a chamber with controlled temperature and humidity using an EM GP grid plunger (Leica, Wetzlar, Germany). The sample dispersion (6 μL) was placed onto an EM grid coated with a holey carbon film (C^{flat}, Protochips Inc., Raleigh, NC, USA). Excess solution was then removed by blotting with a filter paper to leave a thin film of the dispersion spanning the holes of the carbon film on the EM grid. Vitrification of the thin film was achieved by the rapid plunging of the grid into liquid ethane held just above its freezing point. The vitrified specimen was kept below 108 K during storage, transferred to the microscope, and investigated.

Specimens were examined with a Libra 120 Plus transmission electron microscope (Carl Zeiss Microscopy GmbH, Oberkochen, Germany), operating at 120 kV. The microscope was equipped with a Gatan 626 cryotransfer system. Images were acquired using a BM-2k-120 dual-speed on-axis SSCCD camera (TRS).

2.3. Cleaning of substrata

Glass coverslips (Ø 12 mm, Menzel, Braunschweig, Germany) and silicon wafers (Silicon materials, Kaufering, Germany) were cleaned with a solution of NH_4OH (25%), H_2O_2 (35%), and micropure water (1:1:5, v/v/v) at 80°C for 15 min. Afterward, the samples were washed with micropure water (6 × 5 min) and dried with a stream of nitrogen. The gold-coated glass sensor for surface plasmon resonance (SPR, IBIS Technologies BV, Enschede, The Netherlands. 10 × 10 mm^2) were treated by dipping into 0.5 M NaOH in 96% ethanol and followed by rinsing with ethanol (99%) and one last rinsing step with micropure water followed by drying with nitrogen.

2.4. Preparation of polyelectrolyte multilayers

Collagen type I from porcine skin (Mw~ 100 kDa) was provided by Sichuan Mingrang Bio-Tech (Sichuan, China). Native CS A from the bovine trachea (Mw ~ 25 kDa) was provided by Sigma-Aldrich (Steinheim, Germany). Poly (ethylene imine) (Mw~ 750 kDa) was provided by Sigma-Aldrich (Steinheim, Germany). Phosphate-buffered saline (PBS) was prepared according to the following formulation: 2.7 mmol/L KCl, 137 mmol/L NaCl, 1.4 mmol/L KH_2PO_4, 4.3 mmol/L $Na_2HPO_4{\cdot}2H_2O$, pH

7.4. Sodium chloride and acetic acid 30% were purchased from Carl Roth GmbH (Karlsruhe, Germany).

The polyelectrolytes solutions were prepared as follows: PEI was dissolved in 0.15 M sodium chloride solution at a concentration of 5 mg/mL at pH 7.4. CS was dissolved in 0.15 M of sodium chloride at a concentration of 0.5 mg/mL. Collagen I was dissolved in 0.2 M acetic acid at a concentration of 2 mg/mL at 4°C overnight. The final solution of Col I was obtained by diluting the stock solution in 0.2 M acetic acid supplied with 0.15 M sodium chloride at pH 4.

PEM were fabricated on cleaned glass coverslips, gold sensors, and silicon substrates depending on the type of experiment. PEI was used as the first layer to obtain the positive charge on the substrate followed by adsorption of CS as an anionic layer and then Col I as the cationic layer. The multilayer films were fabricated by immersing the glass coverslips in the polyelectrolyte solution for 15 min (PEI, CS) and 20 min (Col I) and one layer of liposomes for 2 h 30 min. By alternating adsorption of CS and Col I, PEM were build up to fourth bilayers named [CS, Col I]$_4$ CS, then the liposomes layer [CS, Col I]$_4$ CS-Lip, and followed by one bilayer [CS, Col I]$_4$ CS-Lip [CS, Col I]$_1$. Each adsorption step was followed by rinsing with 0.15 M sodium chloride solution at pH 4 (3 × 5 min).

2.5. Characterization of polyelectrolyte multilayer and surface properties

2.5.1. Ellipsometry

The thickness of the CS and Col I system was measured by a M − 2,000 V scanning ellipsometer (J.A Woollam Co. Inc., Lincoln, NE) at room temperature as previously described [5]. The measurements were performed at incident angles of linear polarized light of 60 degrees, 65 degrees , 70 degrees, and 75 degrees by M − 2,000 V scanning ellipsometer at ambient conditions, which means that PEMs were dry. The measurements were carried out within a wavelength range of λ = 375–1, 000 nm. The data acquisition rate was about 5 s–10 s per full spectral scan, and the spot size was about ~1–2 mm^2. The experimental data were analyzed with the WVase32 software.

2.5.2. Surface plasmon resonance

The measurements were conducted with an IBIS-iSPR device (IBIS Technologies BV, Enschede, Netherlands). The gold sensor was coated with 11-mercaptoundecanoic acid from Sigma-Aldrich (Steinheim, Germany). The sensor mounted in a flow chamber was equilibrated with 0.15 M sodium chloride to establish a stable baseline. The solutions were injected at a flow rate of 3 μL/s followed by rinsing with sodium chloride for 15 min. PEI was injected for 15 min, followed by CS for 15 min, Col I was injected for 20 min, and the liposomes solution for 150 min. PEM formation was continued until 13 single layers were formed. The average of the angle shifts values (m°) of each rinsing step was used for plotting the graphs.

2.5.3. Zeta potential measurements

The zeta potential of PEM was measured with a SurPASS electrokinetic analyzer (Anton Paar, Graz, Austria). Glass coverslip (10 × 20 mm^2) was cleaned and coated with multilayers and mounted in the gap cell with double-sided tape. 1 mmol/L KCl solution was applied as the model electrolyte, and 0.1 mol/L NaOH was used for pH titration from pH 3.0 to 10 (acid-based pH). The flow rate of 100–150 mL/min at a maximum pressure of 300 mbar was adjusted to determine the zeta potential using the streaming. Each measurement was done in duplicate.

2.5.4. Atomic force microscopy

Atomic force microscopy (AFM, Nanowizard IV, JPK-Instruments, Berlin) in Quantitative Imaging Mode (QI) was performed to investigate the surface roughness and topography. Topographical images were recorded using silicon cantilever (qp-BioT, Nanosensors) in a standard liquid cell (JPK-Instruments) containing distilled water. A force map area of 5 × 5 μm^2 was recorded with a resolution of 512 × 512 pi^2 (pixel). Roughness analysis and calculation of the elasticity were performed using the software JKP Data Processing V5.0.85 and Gwyddion (Gwyddion V2.49, 64-bit).

2.6. Cell culture

Cryopreserved C2C12 myoblasts were thawed and grown in Dulbecco's modified Eagle's medium (DMEM) supplemented with 10% (v/v) fetal bovine serum (FBS), and 1% antibiotic solution (penicillin/streptomycin), all provided by Biochrom AG (Berlin, Germany) in a humidified 5% CO_2/95% air atmosphere. Cells of almost confluent cultures were washed once with sterile PBS followed by treatment with 0.25% trypsin/0.02% EDTA at 37°C for 3 min. Trypsin was neutralized with DMEM with 10% FBS, and the cells were re-suspended in DMEM after centrifugation at 250*g* for 5 min. Finally, the cells were seeded on PEM-coated glass coverslips at a concentration of 4 × 10^4 cells mL^{-1}.

2.7. Viability assay and cell adhesion studies

C2C12 cells were seeded on glass coverslips coated with PEM coating liposomes, or Col I as terminal layers. Cultures were incubated for 24 h, 3 and 7 days, respectively, at 37 °C. After the incubation time the cell viability was determined by QBlue cell viability assay kit (Biochain, Hayward, USA). The cells were washed once with PBS to remove the medium. Then, 500 μL of Qblue solution with colorless medium (10:1) was added to each well and incubated at 37°C for 3 h. Finally, 100 μL of supernatant from each sample was added to black 96 well plate, and the fluorescence intensity was measured at 544 nm excitation and 590 with plate reader.

On the other hand, C2C12 cells were seeded on glass coverslips coated with PEM coatings of either liposome 10th layer, or Col I as terminal layers to evaluate the cell adhesion. PEM-modified glass coverslips were placed into 24 well plates. The re-suspended cells were seeded on the samples in DMEM supplemented with 10% FBS. After incubation at 37°C for 4 h, cells attached to the PEM were fixed with 4% paraformaldehyde solution (Sigma-Aldrich Chemie GmbH, Taufkirchen, Germany) for 10 min. After rinsing with PBS twice, the cells were permeabilized with 0.1% Triton X-100 in PBS (v/v) (Sigma-Aldrich Chemie GmbH, Taufkirchen, Germany) for 10 min. After rinsing with PBS, non-specific binding sites were blocked by incubation with 1% (w/v) bovine serum albumin (BSA, Merck, Darmstadt, Germany) in PBS at room temperature for 1 h. The focal adhesion protein vinculin was stained using a primary mouse antibody (1:100, Sigma) and a secondary Cy2-conjugated goat anti-mouse antibody (1:100, Dianova). The actin cytoskeleton was visualized by incubating the samples with Phalloidin CruzFluor 555 (1:1000, Santa Cruz Biotechnology, Heidelberg, Germany) at room temperature for 30 min. Cell nuclei were visualized by TO-PRO3 (1:500, Invitrogen, Darmstadt, Germany) incubating the samples for 30 min. The samples were washed with PBS and mounted with Mowiol 4–88 (Calbiochem, Darmstadt, Germany) containing 25 mg mL−1 1,4-diazabicyclo [2.2.2]-octane (Carl Roth GmbH & Co. Kg, Karlsruhe, Germany) and examined with confocal laser scanning microscopy (CLSM 701, Carl Zeiss Micro-Imaging GmbH, Jena, Germany) using 10 × , 20 × objectives for quantification of cell adhesion and spreading, while a63 × oil immersion objective was used for higher magnification to visualize nuclei, actin cytoskeleton, and focal adhesions. Images were processed with the ZEN2012 software (Carl Zeiss). The analysis of images to quantify cell count and cell area was performed with Image J.

2.8. Studies on uptake of liposomes and cargo by cells

Quantitative analysis of the uptake of the liposomes was carried out with C2C12 cells plated on glass coverslips coated with PEM consisting terminal liposomes or Col I layers by flow cytometry. After 4 h, the medium was removed, and the samples were washed once with PBS. Afterward, cells were incubated with 0.25% trypsin/0.02% EDTA at 37°C

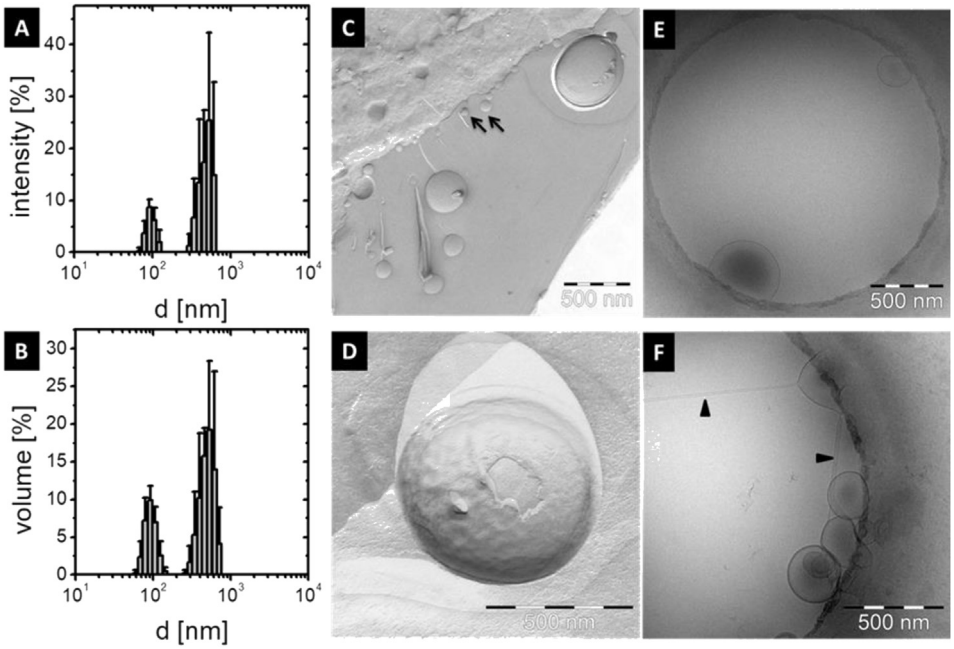

Fig. 2. Characterization of cationic liposomes in acetate buffer pH 4 (10 mM, 0.15 M NaCl). Intensity-weighted **(A)** and volume-weighted **(B)** size distribution curve (mean and standard deviation of three independent liposome preparations) measured by dynamic light scattering. Representative freeze-fracture TEM **(C/D)** and cryo-TEM **(E/F)** micrographs are shown. The bars indicate 500 nm. Arrows indicate small vesicles with a diameter below 100 nm and triangles lipid tubes.

for 3 min. The detached cell suspensions were centrifuged at 200×*g* for 5 min, and the supernatant was carefully removed. Cells for imaging were diluted to a concentration of 1×10^6 cells in 60 μL per sample. Images were acquired using ImageStream® Flow cytometer (Merk, Darmstadt, Germany). The sample was measured with bright field at 60 × magnification, using AMNIS INSPIRED data acquisition software. The bright field was collected on channel 6, SSC on channel 2 (505–560 nm) and 5 (642–745 nm). Only 60 μL of sample was loaded, and 10,000 events meeting the cell classifier were acquired per file at 7 μm core diameter. A bright-field area vs. intensity side scatters plot was used to identify Texas Red and Rhodamine staining.

2.9. Differentiation studies: alkaline phosphatase assay and Alizarin Red-S staining

PEM-modified glass coverslips were placed into 24 well plates. The C2C12 cells were seeded on the samples in basal medium (DMEM supplemented with 10% FBS) (FBS, Biochrom) at a density of 4×10^4 mL^{-1} for 24 h. Then, osteogenic medium or basal medium with the following specifications were added to the samples: $[CS, Col\ I]_6$ (positive control) in **osteogenic medium with** DMEM, 2% FBS, 100 nM Dex, 50 μg/mL ascorbic acid, and 10 mM β- Glycerophosphate, $[CS, Col\ I]_6$ (negative control) in **basal medium** of DMEM supplemented with 2% FBS only, $[CS, Col\ I]_4$-CS-Lip-$[CS, Col\ I]_1$ in osteogenic medium. $[CS, Col\ I]_4$-CS-Lip (DEX)-$[CS, Col\ I]_1$ loaded with Dex-containing liposomes in DMEM 2% FBS, 50 μg/mL ascorbic acid and 10 mM β- Glycerophosphate (no dexamethasone was added to the medium).

Osteogenic medium composition was selected (DMEM 2% FBS, 100 nM Dex, 50 μg/mL ascorbic acid, and 10 mM β- Glycerophosphate promoting osteogenesis of C2C12 cells [34].

After 6 days, the cells were rinsed with PBS, and cell lysis was done using Triton X-100 for 30 min under shaking. Then, 100 μL of cell lysate was incubated with 1 mg/mL of *p*-NPP in 96 well plates and incubated for 90 min at 37°C to estimate expression of alkaline phosphatase (ALP) in C2C12 cells as indicator of osteogenesis. After the incubation time, the measurement of absorbance was done using a plate reader (Fluostar OPTIMA, BMG Labtech) set at 405 nm. At the same time, the BCA protein assay kit (Thermo Scientific, Rockford, IL, USA) was used according to the manufacturer instruction to normalize ALP data to the protein amount, which corresponds to number of cells.

Furthermore, deposition of calcium phosphate as another indicator of osteogenic differentiation of C2C12 was studied. The cells were rinsed with PBS and fixed with 4% paraformaldehyde solution for 15 min. After rinsing with PBS twice, the cells were stained with Alizarin Red S (40 mM) for 30 min at RT. The cells were photographed with a transmitted light microscope after the staining (Nikon ECLIPSE Ti2, Tokyo, Japan) equipped with a CCD camera (DCIN, 12 V, EXT1/0, Tokyo, Japan). Afterward, the samples were rinsed with PBS again, and the presence of calcium deposits stained in red-orange color. For the quantification, the staining was extracted adding 10% acetic acid and neutralized with 10% ammonium hydroxide. The absorbance was measured at 570 nm with a plate reader.

2.10. Statistical analysis

All statistical analyses were performed with Origin 8G software. Means, standard deviations were calculated. Analysis of significance was performed by one-way ANOVA. A value of $p < 0.05$ was considered significantly different indicated by an asterisk. Further, box plots are shown where appropriate. The box indicates the 25th and 75th percentiles, the median (dash) and mean value (black square), respectively.

3. Results and discussion

3.1. Characterization of liposomes

The OO4/DOPE (1/3, n/n) liposomes were characterized regarding their size distribution, morphology, and surface charge at pH 4 in the presence of 0.15 M NaCl, the conditions of PEM formation. In Fig. 2A and B, the intensity- and volume-weighted size distribution curves are depicted, showing two size populations. The intensity-weighted curve results directly from the light scattering measurements, while the volume-weighted results (calculated from the intensity-weighted curve) are more representative than the other due to multimodal size distributions [35]. No particles with diameters above 1 μm were detected. The first size population appears at diameters between 70 nm and 100 nm,

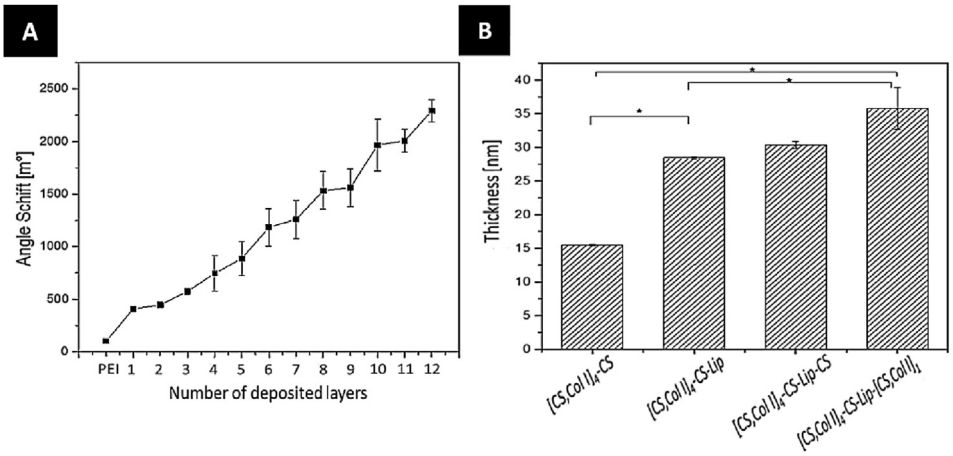

Fig. 3. A) Layer growth of polyelectrolyte multilayer (PEM) systems of [CS, Col I]$_4$-CS-Lip-[CS, Col I]$_1$ by surface plasmon resonance numbered as 1st layer to 12th layer. Odd layer numbers correspond to chondroitin sulfate (CS) coating and even layer numbers correspond to collagen I (Col I) coating except the 10th layer, which corresponds to liposomes (Lip); n = 20, mean ± SD. **B)** Progression of the layer thickness of PEM after adsorption of the final layers of liposomes (Lip), CS and Col I by ellipsometry; n = 10, mean ± SD, *p ≤ 0.05.

and the second with diameter between 300 nm and 700 nm. The population with the larger diameter-size dominates in the intensity- and volume-weighted curves. To obtain information about the morphology of the liposome formulation, TEM was performed with samples treated by freeze-fracture and cryo-preparation (Fig. 2C–F). Freeze-fracture TEM showed liposomes with spherical shape (Fig. 2C and D). Also, small vesicles (Fig. 2C, arrows) next to larger ones with sizes > 300 nm were found that fit to the DLS measurements. However, no exact size determination is possible by this method because the fracture plane can be far away from the center of spherical liposomes. Indeed, the cryo-TEM micrographs show the unilamellar character of the liposomes (Fig. 2E and F). Moreover, tubes are present, which connect different vesicles (Fig. 2F, triangles). This tube formation is an effect of the OO4 lipid with its bulky head group, which can stabilize such highly curved structures [36]. It should be underlined that the tube formation represents not a disadvantage for the embedding process in PEM because not the shape but charge density is important for the adsorption of charged entities during PEM formation [37]. Therefore, zeta potential was measured to confirm the overall charge that liposomes possess in the buffer used in LbL-based PEM formation. The average ζ potential of liposomes was 49.5 ± 4.8 mV. This result indicates a highly positive charged surface, useful as a polycationic component for multilayer formation, as it was shown previously by our group using cationic polymeric particles with a ζ potential of ≈30 mV [38]. A further advantage is that the positive charge also provides colloidal stability in suspension [39]. X-ray diffraction studies demonstrated that OO4/DOPE 1/3 forms non-correlated bilayers even at high lipid concentrations due to electrostatic repulsion [39]. This behavior causes the tendency to form spontaneously unilamellar vesicles. Since previous experiments demonstrated a high affinity of OO4 to membrane material of extruders, an extrusion step was declined to avoid changes of the OO4/DOPE ratio.

3.2. Characterization of multilayers

Multilayer formation of CS and Col I was studied with the optical technique of SPR. SPR was used to investigate the layer growth behavior

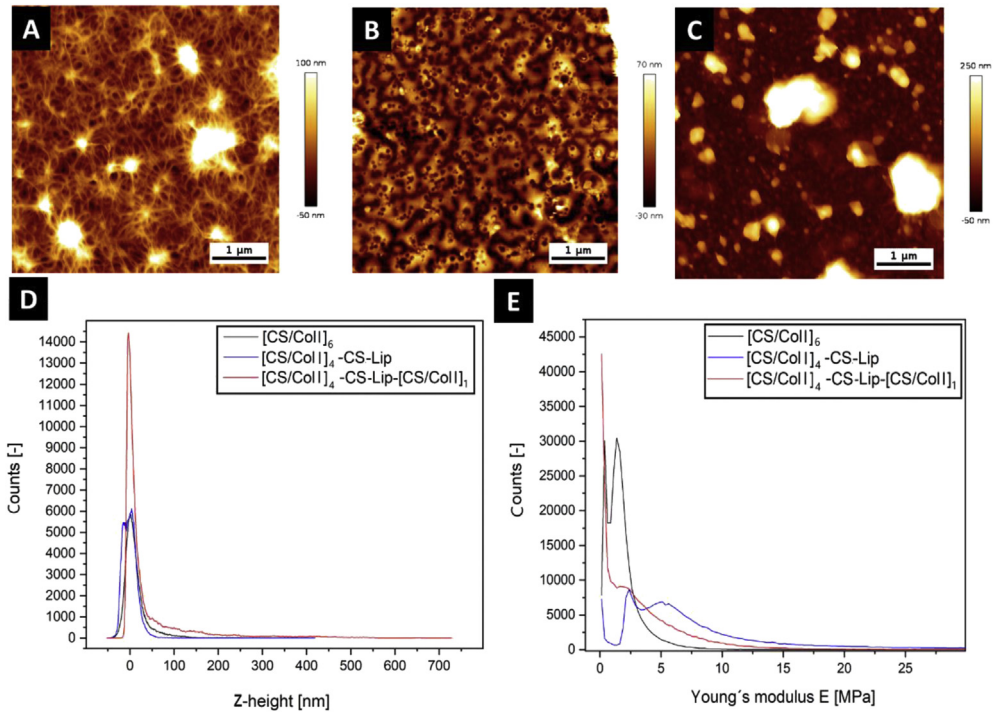

Fig. 4. A-C) Surface topography of **(A)** liposome-free CS and Col I multilayers of the sequence [CS, Col I]$_6$, **(B)** multilayers with embedded liposomes of layer-by-layer sequence [CS, Col I]$_4$-CS-Lip, **(C)** surface topography of [CS, Col I]$_4$-CS-Lip- [CS, Col I]$_1$, by atomic force microscopy [Scale bar: 1 µm]. **D)** Topography height distributions curves of multilayers film. **E)** Distribution curves of E modulus with a force map of an area of 5 × 5 µm^2.

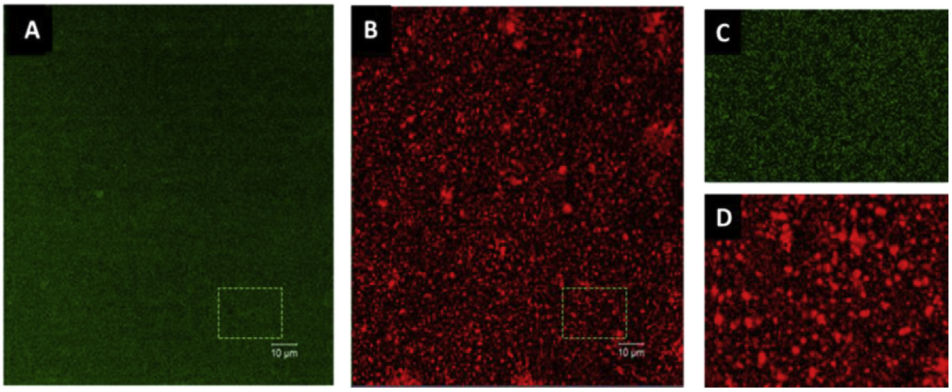

Fig. 5. A) Confocal laser scanning microscopy images of polyelectrolyte multilayer (PEM) system [CS, Col I]$_4$-CS-Lip-[CS, Col I]$_1$ CS was labeled with FITC (green), **B)** liposomes with Rhodamine-DOPE conjugated (red) on PEM [Scale: 10 µm, 63 × magnification].**C/D)** Zoom of CS and liposomes distribution of the area in the white square.

also as an evidence for PEM formation. Fig. 3 (A) shows a linear growth behavior of PEM; every layer deposition increased the angle shift, which corresponds to an increase of the adsorbed mass [17,30]. It was observed that after the 6th layer, Col I contributed more to mass adsorption than CS, which is probably related to the higher molecular weight of Col I, which was well in line with previous studies [17]. Furthermore, the addition of liposomes as 10th layer (PEM sequence [CS, Col I]$_4$-CS-Lip) contributed significantly to mass deposition, which was evident by the largest angle shift of 500 m° compared with the other deposition steps in the LbL sequence shown in Fig. 3 (A). This is probably due to the large size of liposomes compared with that of the polyelectrolytes CS and Col I. To obtain also information on the layer thickness, ellipsometry on silicon substrate was applied to characterize the PEM as shown in Fig. 3 (B). The measurements were performed in duplicate of dry films; data were obtained from five different points on each sample with an area of 1–2 mm^2. The deposition of 9 polyelectrolyte layers (PEM sequence [CS, Col I]$_4$-CS) resulted in a dry film thickness of 15 nm. An increase in thickness by 40 nm was found after liposome adsorption (PEM sequence [CS, Col I]$_4$-CS-Lip), which is another evidence for the deposition of liposomes as part of PEM. The relatively low thickness increase after adsorption of liposomes compared with their size obtained in DLS and TEM measurements is probably due to their drying and shrinking. In addition, ellipsometry is providing an integral measure of thickness, which includes areas of higher (with adsorbed) and lower (without adsorbed liposomes) thickness. The final adsorption of a cover layer on the liposomes composed of CS and Col I (final PEM sequence [CS, Col I]$_4$-CS-Lip-[CS, Col I]$_1$) to an overall thickness of 45 nm. The results of ellipsometry confirmed the increase in mass deposition observed in SPR particularly after addition of liposomes. It should be noted that thickness of hydrated multilayers will exceed that of dry layers, but ellipsometry data revealed that the thickness increase of a single liposome layer is equivalent to that of the preceding 10 single layers of polyelectrolyte macromolecules, which illustrates the major contribution of adsorbed liposomes to the thickness of multilayer films.

Fig. 4 shows the results of AFM studies that shall shed a light on the topography of PEM with incorporated in comparison with the multilayer without liposomes. The deposited polyelectrolytes without liposomes showed a rather homogenous distribution in the scanned areas (Fig. 4A). The LbL sequence [CS, Col I]$_6$ was chosen for this experiment because the number of deposition steps is comparable with that of the liposome-loaded PEM. An assembling into a fibrous network was detected, which can be assigned to Col I. This indicates the fibrillization of the soluble Col I after its deposition, which is most probably due to an interaction with CS supporting arrangement of collagen fibers. Details have been discussed in our previous work [17,30]. Evaluation of AFM images after liposome adsorption [CS, Col I]$_4$-CS-Lip showed a remarkable change in surface topography as demonstrated in Fig. 4 (B). Flattened structures appeared as an indication of presence and deformation of liposomes probably due to the strong electrostatic interaction with the preceding negative-charged CS layer. The spherical shape of liposomes was probably lost (with their flattening on the charged surface, resulting in the elevated structures). Fig. 4 (C) shows the topography after adsorption of the terminal CS, Col I bilayer. The images are quite different from previous liposome layer with larger aggregates that might indicate that the presence of liposomes in a kind of random distribution may provide nucleation sites for subsequent adsorption of CS and Col I, leading to an accumulation of these polyelectrolytes in certain areas. However, it is also visible that there is a rather granular morphology of multilayer as seen in previous studies with CS and Col I, when the protein was only used as terminal layer [40]. This means that the fibrillization of collagen is a process that requires the presence of multiple layers of the protein in the PEM.

Fig. 4 (D) shows height distribution curves of the highest and lower points in the measured area (5 × 5µm^2), which is another measure of overall roughness of the multilayer surface. Here, the highest frequency peak is found after the embedding of the liposomes, which can be taken as another evidence for their immobilization. It is also interesting to note that the preceding [CS, Col I]$_6$ and the final CS, Col I]$_4$-CS-Lip- [CS, Col I]$_1$ As supplemental information about the mechanical properties, Young's modulus (E) was measured. Fig. 4 (E) the E modulus of the sequence [CS, Col I]$_6$ was ~3 MPa. The mean E modulus after embedding the liposomes with sequence [CS, Col I]$_4$-CS-Lip shows the incidence of two peaks; the first peak was around~4 MPa that indicates the presence of the previous layers as Col I. The second peak ~ 6 MPa resembles most probably the liposomes that can show extremely high E moduli after adsorption on surfaces as found in previous studies [41]. The adsorption of the terminal [CS, Col I] bilayer is represented by peak of ~4 MPa like the one of the initial [CS, Col I]$_6$ multilayers but with a wider distribution. This indicates also a complete coverage of the liposomes layer because of the similar value like the PEM before liposome adsorption. The description of the mechanical properties visualized in Figure D/E corresponds to the images that can be found in the supplemental information (S1).

From AFM, it was assumed that elevations and changes in the roughness of the [CS, Col I]$_4$-CS-Lip- [CS, Col I]$_1$ films represent liposomes. To proof that liposomes are embedded or part of multilayers CLSM studies were performed using FITC-labeled CS and Rhodamine-DOPE labeled OO4/DOPE liposomes for the formation of [CS, Col I]$_4$-CS-Lip- [CS, Col I]$_1$ PEM. Fig. 5(A) shows that a homogeneous distribution of FITC-CS was observed. Fig. 5(B) shows the distribution of Rhodamine-DOPE fluorescence across the PEM, indicating a successful incorporation of the positively charged labeled liposomes. The image indicates a homogenous distribution of liposomes over the whole area (see Fig. 5C and D), sometimes that may represent some aggregates. The

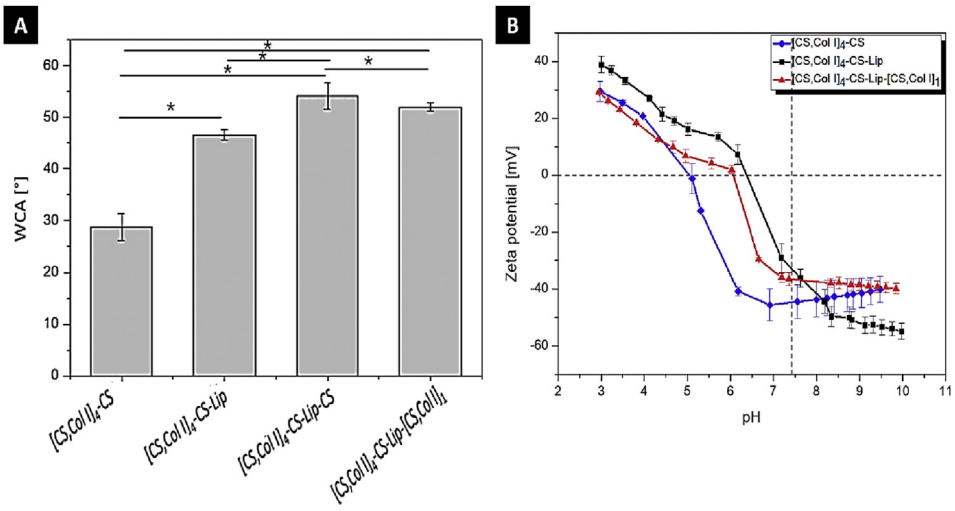

Fig. 6. A) Static water contact angle measurement during multilayer formation after nine layers. Results are means ± SD of three independent experiments. **B)** Zeta potential measurements of the three different multilayers. Results are means ± SD of two independent experiments.

dimensions of items are related to the size area of liposomes and fit to the area of the elevations found in AFM.. Furthermore, the [CS, Col I]$_4$-CS-Lip PEM were prepared in a black, flat bottom 96-well plate to measure the loading degree by fluorescence measurements in a plate reader. It turned out that approximately 10% of the liposomes from the fluid phase were immobilized during the incubation process. Quantification of fluorescence yielded that approximately 15 μg/cm^2 liposomes are bound in a single well of 96 well-plate. The graphical evaluation of Fig. 5B provides the information that about 20% of the investigated film area are covered with Rhodamine-DOPE labeled liposomes. The image for the relative area can be found in the supplemental information (S2).

Surface wettability is an essential factor in the characterization of multilayers because the wetting properties control protein adsorption, and subsequently cell attachment [42]. In addition, wetting properties can be also used to follow the process of multilayer formation because of differences in wetting properties of the different polyelectrolytes [17,30]. Wetting characteristics of [CS, Col I]$_4$-CS-Lip-[CS, Col I]$_1$ films and intermediate processing steps are presented in Fig. 6A. The film with the sequence [CS, Col I]$_4$-CS (basal film for adsorption of cationic liposomes) is more hydrophilic with a WCA of 30°. CS is known to be a hydrophilic polysaccharide, therefore, the contact angle was lower in comparison to Col I [17]. After adsorption of liposomes, the WCA measurements of [CS, Col I]$_4$-CS-Lip yielded a higher contact angle of 45 degrees, which corresponds to moderately wettable surface. The CLSM experiments above demonstrated an incomplete coverage with liposomes (see Fig. 5), which indicates that both OO4/DOPE liposomes and uncovered CS contribute to this WCA value. With addition of a CS cover layer (PEM sequence [CS, Col I]$_4$-CS-Lip-CS), the WCA increased to 57°. Theoretically a decrease was expected after addition of a CS layer. The observed increase from 45° to 55° may result from a reorganization of the liposome (layer) after interaction with CS and is also a hint for intermingling structures of liposomes and CS on the surface of [CS, Col I]$_4$-CS-Lip-CS system. The final system [CS, Col I]$_4$-CS-Lip- [CS, Col I]$_1$ has a comparable WCA. These measurements revealed that the [CS, Col I]$_4$-CS-Lip- [CS, Col I]$_1$ represent a moderately wettable surface. In a previous work, we showed a WCA of ≈45° for a [CS, Col I]$_4$ PEM system [30]. The slightly higher value of ≈50° detected for the system [CS, Col I]$_4$-CS-Lip-[CS, Col I]$_1$ is probably related to intermingling of liposomes with the other two polyelectrolytes.

Zeta potential titration measurements were carried out because of the impact on surface charge on protein adsorption and cell adhesion [43] but also to follow the changes in surface potential with the final adsorption steps of liposomes, CS and Col I. Fig. 6 (B) shows the changes of the zeta potential during the titration from acidic to basic pH for the basal PEM system [CS, Col I]$_4$-CS (CS before liposome attachment), [CS, Col I]$_4$-CS-Lip and the fully assembled liposome-loaded PEM system [CS, Col I]$_4$-CS-Lip-[CS, Col I]$_1$ that all resulted in a sigmoidal zeta potential curve.

The film with the terminal CS layer, [CS, Col I]$_4$-CS, has a point of zero charge (PZC) at pH 5 and shows a negative zeta potential with values around −40 mV at pH 6 lower, which shows the acidic character of the CS, because of the presence of sulfate groups and deprotonated carboxylic groups of CS that have a pKa value of around 3. Therefore, the surface charge is dominated by the terminal CS layer, which covers the film surface. The addition of cationic liposome, LbL sequence [CS, Col I]$_4$-CS-Lip, results in a PZC at higher pH values (around pH 6) due to the primary amino functions in the head group. In a previous work the pKa of OO4 was determined at pH 6 [27], this means that more than 99% of the lipid species are uncharged at pH ≈ 8. The observed shift in the PZC also supports that liposomes were irreversibly adsorbed on the surface and do not desorbing during the washing steps with NaCl. However, the curve also demonstrates that the surface is only partially covered by the liposomes, only. Due to the amino groups of OO4 with a pKa value ≈ 6 a nearly neutral surface would be expected at pH values between 7 and 8 (90–99% neutral NH_2 groups), if the surface is dominated by the liposomes. If, we consider that the NH_2 species in DOPE has a pKa between 7 and 8 [44], a slightly negative zeta potential can be assumed at pH 8–9 (90–99% neutral NH_2 groups, and negatively charged phosphate). Hence, the zeta potential is with values between −40 and −60 mV highly negative at pH values above 7, an additional strong influence of the CS layer below can be assumed, a fact that is conform with the incomplete coverage of the film by liposomes confirmed by CLSM. For the final PEM, [CS, Col I]$_4$-CS-Lip-[CS, Col I]$_1$, a PZC at around pH 6 was detected. This value is slightly below the values determined for the liposome-terminated film [CS, Col I]$_4$-CS-Lip. Possibly, the fact is that the collagen contains less basic side groups such as lysine compared with the OO4/DOPE liposomes can explain this behavior. Nevertheless, additionally the influence of CS can be seen due to the zeta potential of ~ -40 mV above pH 7. Some authors suggested that the values of the zeta potential of the polyelectrolyte films not only reflect the outermost polyelectrolyte layer but as well the composition of the layers nearer to the surface [17], a

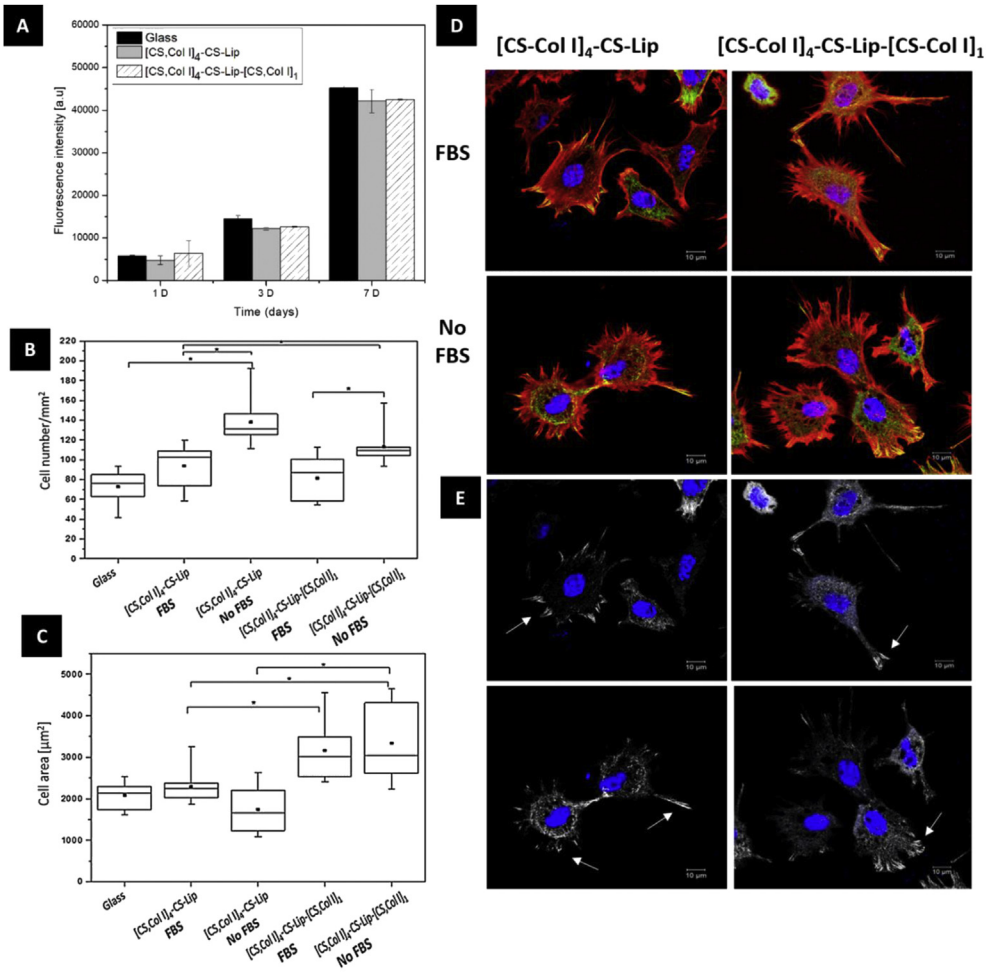

Fig. 7. A) Viability of C2C12 seeded in the presence or absence of bovine serum (FBS) on multilayers [CS, Col I]$_4$-CS-Lip and [CS, Col I]$_4$-CS-Lip-[CS, Col I]$_1$ measured by the QBlue assay for studying of viability of C2C12 cells after 24 h, 3 and 7 days (means ± SD). **B)** Quantification of cell count per square millimeter and **C)** cell spreading area (µm^2) on each of the multilayers after 4 h (Box plots with whiskers, representing first and third quartiles, medians and means, respectively). (*) Statistically significant with p value $\leq$ 0.05. **D)** Merged confocal laser scanning microscopy image of adherent C2C12 cultured on the different PEM after 4 h of incubation in serum and serum-free medium. The cells are stained for filamentous actin (red), vinculin (green), and nucleus (blue). [Scale: 10 µm, 63 × magnification]. **E)** In the lower micrographs, white arrows show vinculin (white) positive focal adhesions for the same cells like above.

fact that fits with our observations. For that reason, it is the dominance of the CS on the PEM surface charge, which indicates that it is moderately present at the surface of the film or that there is an intermingled structures of the outer PEM layers.

3.3. Cell viability and adhesion studies on polyelectrolyte multilayer

PEM of Col I and CS were used to mimic the ECM of bone as it was done in a previous study promoting osteogenic differentiation of mesenchymal stem cells [17]. In this study, C2C12 mouse myoblast cells were used to study biocompatibility and osteogenic potential of the different PEMs because of their ability to differentiate either into myotubes or osteoblast [45]. First cell studies were designed to investigate the effect on viability and cell adhesion of the cationic liposomes embedded into PEM.

The viability of C2C12 on [CS, Col I]$_4$-CS-Lip and [CS, Col I]$_4$-CS-Lip [CS, Col I]$_1$ was studied after periods of 1, 3, and 7 days. Fig. 7A, shows the metabolic activity of C2C12 myoblast studied with Qblue assay that provides a measure of the quantity of viable, metabolic active cells on the different PEMs. The positive control (glass) shows a higher fluorescence intensity, compared with [CS, Col I]$_4$-CS-Lip and [CS, Col I]$_4$-CS-Lip-[CS, Col I]$_1$ after 3 and 7 days. Nevertheless, both PEMs express similar fluorescence intensities, which are not significantly different from the control. Also, the data show an increase of the fluorescence intensity with time due to the growth of cells that indicate a good biocompatibility of PEM also with the cationic liposomes, while a good biocompatibility of the terminal CS-Col I bilayer was expected as found in our previous studies [17]. These results demonstrate that none of the surfaces has any toxic effect, owing to the liposome composition and biocompatible nature of the polyelectrolytes.

The cell adhesion studies were carried on to study cell spreading for the quantification of the cell area, cell number including visualization of actin filaments (red staining), focal adhesions like vinculin (yellow staining), and nuclei (blue staining). These studies are important since cell adhesion and spreading are tightly connected to cell differentiation due to chemical and mechanical signal transduction through focal adhesions including integrins and cell cytoskeleton [46]. C2C12 were seeded in the presence or absence of serum to study cell adhesion on the intermediate PEM with liposomes on terminal layer [CS, Col I]$_4$-CS-Lip and the final PEM [CS, Col I]$_4$-CS-Lip-[CS, Col I]$_1$, In Fig. 7B and C, the results show that there were significantly more cells adhering on [CS, Col I]$_4$-CS-Lip and [CS, Col I]$_4$-CS-Lip-[CS, Col I]$_1$ in the absence of serum, which indicates that adsorption of serum proteins such as albumin on the surface reduces cell adhesion slightly [47], possibly reducing the positive surface charge of liposome terminal layer or the interaction of cell surface integrins with collagen. The analysis of cell spreading data revealed a significantly higher spreading area for cells on [CS, Col I]$_4$-CS-Lip-[CS, Col I]$_1$ in the presence and absence of serum compared with C2C12 cells on films with liposomes as terminal layer. Indeed, the concept to add two layers more after [CS, Col I]$_4$-CS-Lip was not only to protect liposomes from degradation but also to improve the cell adhesion due to integrin-linked adhesion mechanism [7,13]. The advantage of using Col I as a terminal layer is that it provides structural support to cells and cell surface receptors that are important for cell-substrate interaction, for example, via integrin α2β1 receptor of collagen I [48]. In Fig. 7D and E, the organization of the actin fibers in C2C12 seeded on [CS, Col

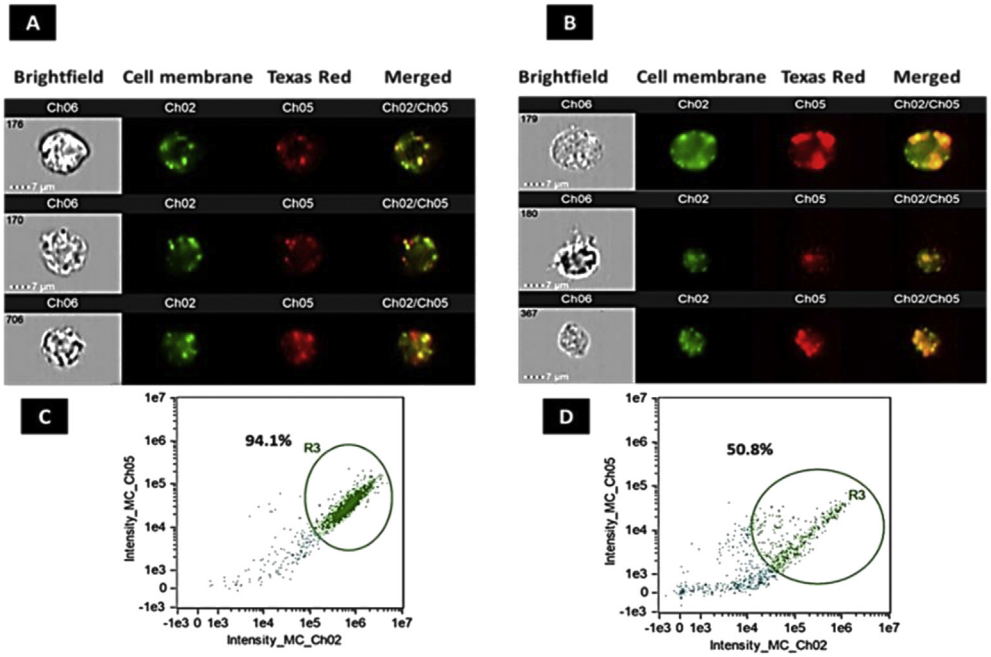

Fig. 8. A/B) Representative images captured by AMNIS ImageStream® Flow cytometer of cells seeded onto multilayers and liposomes with Texas Red dextran after 4 h. The first column shows bright field images of C2C12; the second column shows cell membrane with DiO staining (green); the third column shows liposomes with Texas Red (red); and the last one shows the internalization of Texas Red. [Scale: 7 μm, 60 × magnification]. **A/C)** Polyelectrolyte multilayer with liposomes in the supernatant **B/D)** [CS, Col I]$_4$-CS-Lip-[CS, Col I]$_1$ liposomes with Texas Red dextran. **C/D)** Scatterplots of cell classification into a positive (R3) population.

I]$_4$-CS-Lip was oriented in an irregular form and organized mostly circumferentially independent whether FBS was present or not. In the case of [CS, Col I]$_4$-CS-Lip-[CS, Col I]$_1$ the organization of actin fibers was arranged longitudinally corresponding to higher cell spreading. Furthermore, the staining of vinculin at the end of actin fibers was present in C2C12 cells seeded on both surfaces indicating the presence of focal adhesions reflecting an integrin-mediated interaction with the surface (Fig. 7 E) [48]. The presented cell adhesion studies underline the beneficial effect of Col I as the terminal surface layer but also that the adsorbed liposomes possess an excellent biocompatibility as found in our previous studies [27,28].

3.4. Studies on endocytosis of liposomes labeled with model compounds

The question arose whether PEM-embedded liposomes can deliver a cargo into the cells growing on the modified surface. From our previous studies, it is known that cells have the capacity to rearrange PEMs consisting of CS and Col I mechanically and enzymatically [17], which means that liposomes even embedded underneath a terminal CS-Col I bilayer should be accessible to cells to be taken up by endocytosis. For that purpose, two model compounds were chosen, Rhodamine-DOPE, an amphiphilic compound, which was incorporated in the lipid bilayer of liposomes, and Texas Red dextran as a hydrophilic compound encapsulated in the liposomal aqueous core [49]. Imaging flow cytometry was

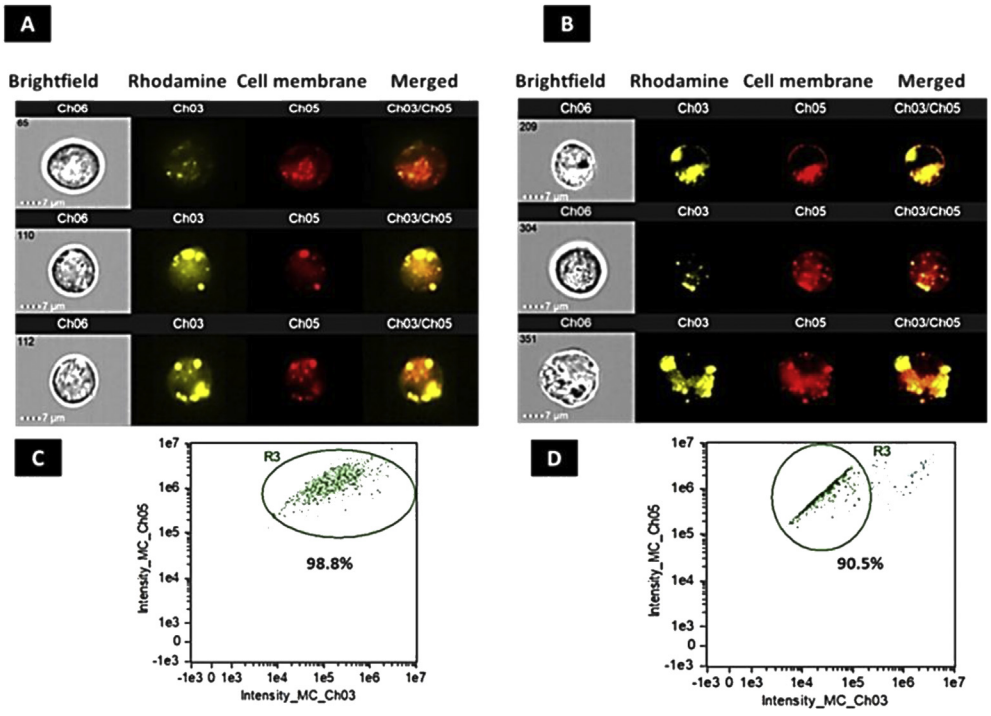

Fig. 9. A/B) Representative images captured by AMNIS ImageStream® Flow cytometer of cells seeded onto multilayers [CS, Col I]$_6$ supernatant and [CS, Col I]$_4$-CS-Lip-[CS, Col I]$_1$ with Rhodamine-DOPE conjugate after 4 h. The first column shows bright-field images of C2C12; the second column shows liposomes with Rhodamine-DOPE conjugate (yellow); the third column shows cell membrane with Cell Mask staining (red); and the last one shows the internalization of Rhodamine-DOPE conjugated. [Scale: 7 μm, 60 × magnification]. **A/C)** polyelectrolyte multilayer (PEM) with liposomes in the supernatant **B/D)** Liposomes embedded in PEM [CS, Col I]$_4$-CS-Lip-[CS, Col I]$_1$. **C/D)** Scatterplots of cell classification into a positive (R3) population.

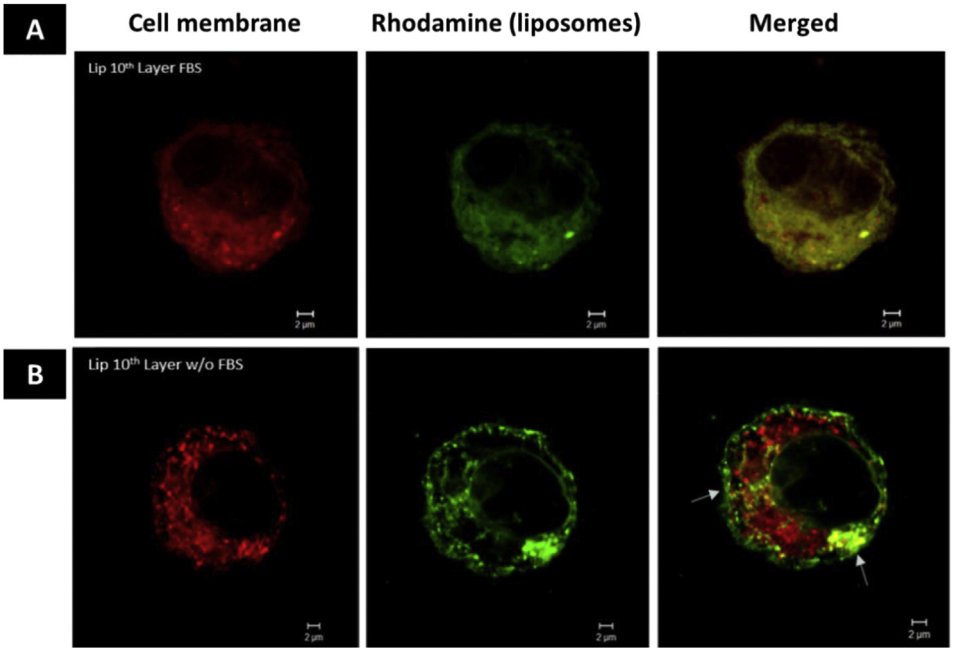

Fig. 10. Confocal laser scanning microscopy images of C2C12 cells growing on [CS, Col I]$_4$-CS-Lip-[CS, Col I]$_1$ in the presence of fetal bovine serum and under serum-free conditions. Cell membrane Cellmask Red (red), liposomes labeled with Rhodamine-DOPE conjugate (green). [Scale: 2 μm] Arrows point to co-localization sites of the liposomes.

used to investigate and quantify cells, which were labeled with one of the fluorescent labels after growing on [CS, Col I]$_4$-CS-Lip-[CS, Col I]$_1$ in comparison with cells growing on [CS, Col I]$_6$ with OO4/DOPE liposomes in the supernatant as a control. An association of the labeled compounds with the cells was taken as a strong indication of endocytic uptake of liposomes. Fig. 8 shows the quantification of Texas Red dextran-positive C2C12 cells. The micrographs visualized that a positive Texas Red signal is strongly associated with the cells (Fig. 8A and B). The intensity was shifted to higher values, indicated by the area (R3) after successful uptake of Texas Red dextran (Fig. 8C and D). The quantification of liposome uptake (Texas Red dextran-positive cells) indicated that for cells that grow on the liposome-loaded PEM [CS, Col I]$_4$-CS-Lip-[CS, Col I]$_1$ 50.8% of the cells internalized liposomes (Fig. 8B, right diagram). However, for cells growing on a liposome-free PEM film [CS, Col I]$_4$ with liposomes in the supernatant, 94.1% C2C12 cells were Texas Red dextran-positive. The physical studies on multilayer formation indicated that structural rearrangement processes the liposomes when a further CS layer was added (see results of WCA studies). Therefore, some loss of the hydrophilic cargo seems to be possible after the adsorption of liposomes. Hence, the uptake result from adsorbed liposomes labeled with Texas Red-dextran seems to be encouraging because they demonstrate that a transfer of hydrophilic substances is possible with this system.

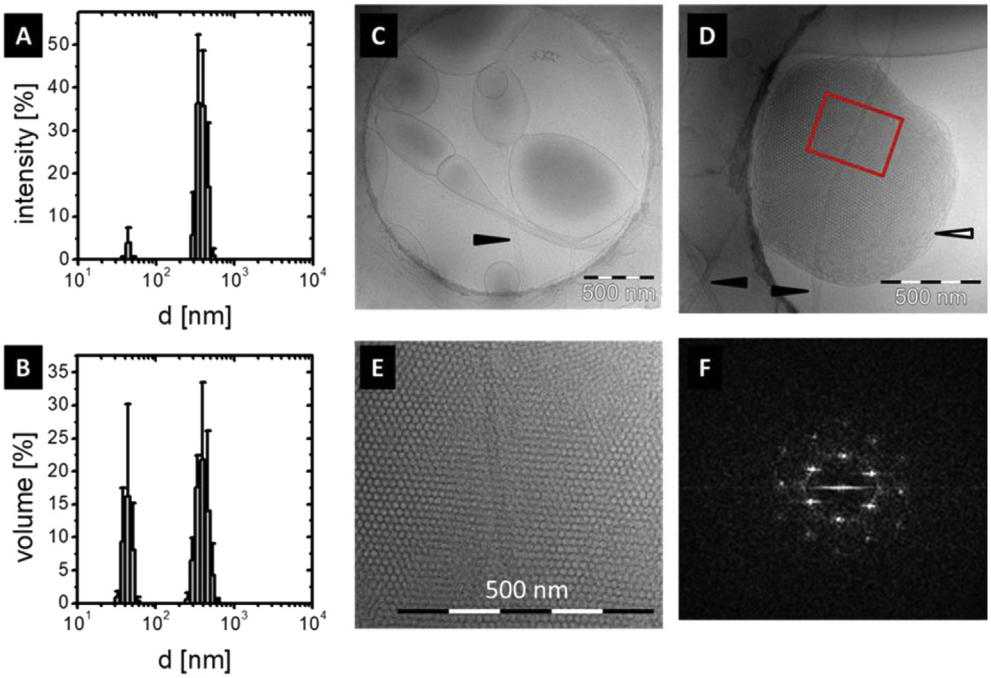

Fig. 11. Characterization of cationic liposomes in acetate buffer pH 4 (10 mM, 0.15 M NaCl) loaded with dexamethasone (2.5% m/m). Intensity-weighted **(A)** and volume-weighted **(B)** size distribution (mean and standard deviation of three independent liposome preparations) measured by dynamic light scattering. Representative cryo-TEM **(C–E)** micrographs are shown. The bars indicate 500 nm. Black triangles indicate lipid tubes and white triangles, cubosomes. **E)** is the zoomed image in the red labeled region of Figure **D**. **F)** shows the diffractogram gained by D due to Fourier transformation demonstrating the high order of the cubic structure.

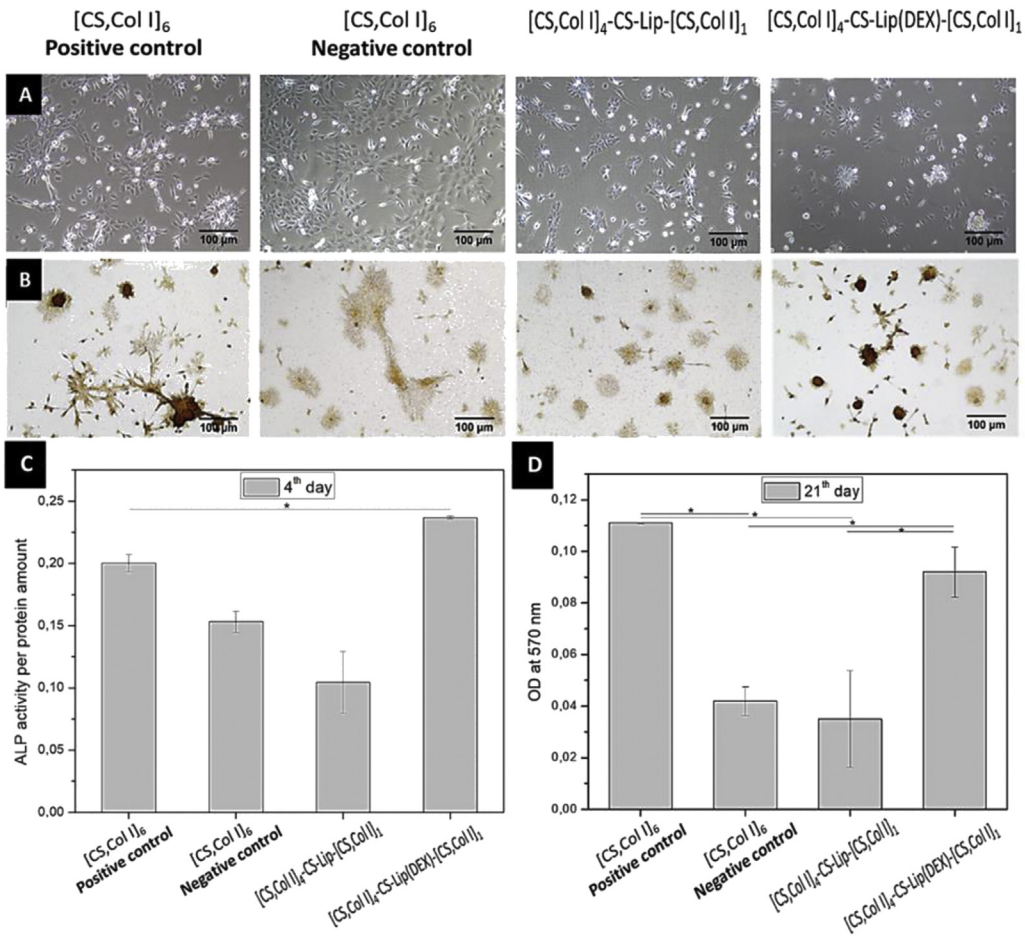

Fig. 12. Four systems are compared for osteogenic differentiation: [CS, Col I]$_6$ in osteogenic medium (positive control), [CS, Col I]$_6$ in basal medium (negative control), Dex-free liposomes [CS, Col I]$_4$-CS-Lip-[CS, Col I]$_1$ in osteogenic medium and loaded with Dex-containing liposomes [CS, Col I]$_4$-CS-Lip(DEX)-[CS, Col I]$_1$ in basal medium with (ascorbic acid and β- Glycerophosphate). **A)** Phase contrast images of C2C12 on the different systems after 4 days. **B)** Alizarin Red-S staining after 14 days [Scale: 100µm, 10 × magnification]. **C)** Measurements of ALP activity in C2C12 cells seeded the different conditions in 24 well plates after 4 days of incubation. The measurements were normalized to the protein amount using the BCA assay. **D)** Measurement of Alizarin Red staining after 14 days of incubation.

Fig. 9 shows the uptake of Rhodamine-DOPE conjugate in C2C12 cells growing either on the liposome-loaded film [CS, Col I]$_4$-CS-Lip-[CS, Col I]$_1$ or[CS, Col I]$_6$ with liposomes in the supernatant. The Rhodamine-DOPE label was detected in C2C12 cells growing on both systems. The quantification of liposome uptake indicated that 90.5% of cells growing on [CS, Col I]$_4$-CS-Lip-[CS, Col I]$_1$ were Rhodamine-DOPE-positive (Fig. 9D), whereas 98.8% of cells growing on [CS, Col I]$_6$ with liposomes in the supernatant, were Rhodamine-DOPE positive (Fig. 9C). Consequently, an efficient uptake of liposomes can be assumed for both conditions.

Summarizing the observations above, it can be demonstrated that C2C12 cells efficiently internalize hydrophilic or lipophilic substances from liposomes embedded in [CS, Col I]$_4$-CS-Lip-[CS, Col I]$_1$ PEM. It cannot be differentiated with this experiment, if complete liposomes or only the cargo is taken up, although the first case is more reasonable. The results also indicate that uptake of cargo by C2C12 cells from liposomes in the supernatant is more efficient than from those embedded in multilayers, particularly regarding hydrophilic cargo. The small differences in the transfer of Rhodamine-DOPE between adsorbed and supernatant liposomes indicate that embedded liposomes remain accessible and can be taken up by adhering C2C12 cells. However, the postulated rearrangement of liposomes that is indicated by WCA and ellipsometry measurements might be connected to increased permeabilization of the lipid bilayer and partial loss of the hydrophilic cargo Texas Red dextran from the core of liposomes, while the lipophilic cargo Rhodamine-DOPE is an intrinsic part of the lipid membrane and remains in the hydrophilic environment. Hence, a different efficiency in the transfer of hydrophilic and lipophilic cargo can be expected.

To obtain more information if the cell-associated fluorescence found by flow cytometry analysis was related to internalization by or only association of liposomes with the cells, uptake experiments were performed with C2C12 cells growing on [CS, Col I]$_4$-CS-Lip-[CS, Col I]$_1$ using Rhodamine-DOPE-loaded liposomes in the presence and absence of serum using CLSM. Bovine serum was added here to mimic the presence of plasma and subsequent adsorption of proteins on the PEM surface that may affect also the interaction of cells with embedded liposomes. Fig. 10 shows that in both cases, the label was found intracellularly in a granular distribution although more when FBS was absent proving the endocytosis of liposomes with transfer of the cargo into the cell.

3.5. *Proof of concept study with dexamethasone-loaded liposomes*

The previous results demonstrated clearly that the novel cationic OO4/DOPE liposomes embedded in a PEM system can be used for controlled release or transfer of components into cells. However, as a proof-of-concept that such transfer can also change cellular functions, the effect of the internalization of a lipophilic drug with effect on cell differentiation is studied here. For this purpose, dexamethasone (Dex) was incorporated in the lipid bilayer of liposomes to induce differentiation of C2C12 cells into osteoblasts [50]. The quantification of the loading capacity by HPLC demonstrated an efficient loading of 2.5% (m/m) of dexamethasone (loading efficiency of 54.0% and 54.3% in an experimental duplicate with a theoretical 5% (m/m) loading). The incorporation of dexamethasone in the lipid bilayer had only slight effects on OO4/DOPE liposomes. The size distribution curve (Fig. 11A and B) shows still a bimodal distribution comparable with drug-free OO4/DOPE liposomes (Fig. 2A and B). However, compared with the drug-free liposomes, the smaller population decreased in intensity. Consequently, a slight increase in the particle size was observed. The measured ζ potential decreased from 49.5 ± 4.8 mV to 44.1 ± 4.2 mV. However, it was still highly positive, which guarantees the adsorption during LbL multilayer

formation. Furthermore, large unilamellar vesicles and tubular structures were found (Fig. 11C) comparable with unloaded liposomes. Besides, these expected structures, cubosomes appeared, lipid nanoparticles consisting of continuous periodic membrane lattice structures in the inner core (Fig. 11D, white arrows, detail in Fig. 11E). These ordered 'membrane folding', which is connected with an increase of membrane area, allows a high degree of incorporation of lipophilic drugs compared with unilamelar liposomes of comparable size. The treatment of the cryo-TEM micrographs of the cubosomes with Fourier transformation resulted in a reflex pattern of multiple signals, which demonstrates the highly ordered symmetry of the cubic liquid crystalline phase inside the cubosomes (Fig. 11F) [51]. More details about the cubosomes can be found in the supplemental information (S3–S6).

Since, a successful incorporation of dexamethasone in OO4/DOPE liposomes could be shown, their effect after incorporation in [CS, Col I]$_4$-CS-Lip-[CS, Col I]$_1$ on osteogenic differentiation of C2C12 cells was studied regarding the enzymatic activity of ALP and deposition of calcium phosphate by histochemical staining with Alizarin Red. Indeed, this experimental model for osteogenesis of cells induced by other types of Dex-loaded liposomes was demonstrated previously, but applying them in supernatant [51]. The PEM with empty liposomes was chosen for comparison because CS and Col I containing multilayers may promote osteogenic differentiation of cells by mimicking the ECM composition of bone [17]. C2C12 were seeded on the different surfaces as described in the method section. Fig. 12A shows representative phase contrast micrographs of C2C12 cells on the different systems at day 4. It is visible that more cells were found on negative and positive controls that resemble [CS, Col I]$_6$ PEM with osteogenic and basal medium, while cell number on multilayers with embedded liposomes was slightly lower, which corresponds also to the studies with QBlue assay shown in Fig. 7A. Another interesting finding was that C2C12 cells tended to form aggregates when cultured on PEM with Dex-loaded nanoparticles [CS, Col I]$_4$-CS-Lip (DEX)-[CS, Col I]$_1$ (see Fig. 12A again, right micrograph). Alizarin Red-S staining was used to detect the formation of mineralized matrix by C2C12 cells after 14 days. In Fig. 12B, cells growing on [CS, Col I]$_4$-CS-Lip-[CS, Col I]$_1$ loaded with Dex-containing liposomes are characterized by stronger staining with Alizarin Red-S in comparison with the [CS, Col I]$_4$-CS-Lip-[CS, Col I]$_1$ film bearing drug-free liposomes and have a staining that is comparable with the positive control with dexamethasone in osteogenic medium. Quantitative measurements of osteogenic differentiation by ALP activity were done after 4 days and shown in Fig. 12C. An increase of ALP was found in samples where Dex-loaded liposomes were embedded [CS, Col I]$_4$-CS-Lip-[CS, Col I]$_1$ in comparison with the positive and negative control. It was also found that ALP was lower when cells were cultured on PEM with drug-free liposomes [CS, Col I]$_4$-CS-Lip-[CS, Col I]$_1$. Quantification of calcium phosphate by solubilizing bound Alizarin Red is shown in Fig. 12D. It is visible that deposition of calcium phosphate after 14 days was highest in cultures of cells on positive control, followed by cells growing on PEM with Dex-loaded PEM. Both negative control and PEM with drug-free liposomes had significantly lower values of Alizarin Red, which underlines the promoting effect of dexamethasone on differentiation of C2C12 myoblasts into osteoblastic cells.

The results indicate that dexamethasone can be taken up from liposomes embedded in PEM by adhering and growing C2C12 myoblasts cells. Therefore, such multilayer system such as [CS, Col I]$_4$-CS-Lip-[CS, Col I]$_1$ can help to avoid systemic effects, minimizing exposure of healthy or other tissues to the drugs having a local effect, only when used as a coating on implants or scaffold materials [10]. Here, the [CS, Col I]$_4$-CS-Lip(DEX)-[CS, Col I]$_1$ with Dex-loaded liposomes induced the osteogenic differentiation of C2C12 cells.

4. Conclusion

This work has shown that the LbL technique can produce multifunctional surface coatings to tailor the composition and physicochemical properties of surfaces and permit controlled transfer of compounds. The characterization studies demonstrated a stable, relatively uniform film formation with immobilization of liposomes that could be taken up by cells even when covered with an additional bilayer of CS-Col I. Indeed, it was found that the transfer of lipophilic model compounds contained in the lipid bilayer was more efficient than that of hydrophilic contained in the core of liposomes, probably related to the reorganization of liposomes during adsorption of multilayers. It was also possible to demonstrate the functionality of this transfer of compounds by/through immobilized liposomes shown by the effect of a functional cargo like dexamethasone inducing osteogenic differentiation of C2C12 cells in situ. It should be considered that the suggested approach is applicable to a variety of cargos such as drugs, siRNA, mRNA and DNA for gene silencing, transient or permanent gene expression for in situ transfer avoiding potential problems in vivo like systemic toxicity, aggregation/interaction of liposomes with body fluids like blood and removal by the RES ending up in the liver, spleen, and other organs. Hence, the benefit of immobilization of liposomes in PEM is the increase in the uptake efficiency by increasing the local concentration close to the cell but probably also prolonging the half-life of the incorporated compounds. Results can be considered as a proof of concept of combination of LbL systems with liposomes to design the microenvironment of cells by the composition of multilayers and the kind of cargo to have the desired effects on the surrounding cells and tissues.

Author contributions

Y.A.B.B performed large part of surface characterization, studies with cells and writing of the manuscript; G.H. performed transmission electron microscopy, M.M. and C.E.H.S, carried out atomic force microscopy studies and made corresponding contributions to the manuscript. E.L. and K.M. performed high-performance liquid chromatography analysis of dexamethasone content of liposomes and made corresponding contributions to the manuscript. C.W. performed synthesis of lipids, preparation, and characterization of liposomes and was involved in conceptualization of the study and writing of the manuscript. T.G. was involved in conceptualization and writing of the manuscript. All authors were involved in reviewing and editing the final manuscript.

Funding

Y.A.B.B supported by the CONACYT-México and German Academic Exchange Service (DAAD). The work was supported by the Fraunhofer Internal Programs under Grant No. Attract 069–608203 (C.E.H.S.). The supported by the Deutsche Forschungsgemeinschaft (DFG) project-ID 396823779 (C.W.) is acknowledged. T.G. acknowledges the High-Performance Center Chemical and Biosystems Technology Halle/Leipzig and support by the European Regional Development Fund (ERDF).

Declaration of competing interest

The authors declare that they have no known competing financial interests or personal relationships that could have appeared to influence the work reported in this paper.

Acknowledgments

The authors thank the technical assistance of Mrs. Marlis Porobin for performing zeta potential measurements. We are very thankful to Dr. Alexander Navarrete Santos for his help during imaging flow cytometry measurements and data analysis.

Appendix A. Supplementary data

Supplementary data to this article can be found online at https://doi.org/10.1016/j.mtbio.2020.100071.

References

[1] K.M.R. Nuss, B. von Rechenberg, Biocompatibility issues with modern implants in bone - a review for clinical orthopedics, TOORTHJ 2 (2008) 66–78, https://doi.org/10.2174/1874325000802010066.

[2] S.P. Adiga, C. Jin, L.A. Curtiss, N.A. Monteiro-Riviere, R.J. Narayan, Nanoporous membranes for medical and biological applications, Wiley Interdiscip Rev Nanomed Nanobiotechnol vol. 1 (2009) 568–581, https://doi.org/10.1002/wnan.50.

[3] G. Altankov, K. Richau, T. Groth, The role of surface zeta potential and substratum chemistry for regulation of dermal fibroblasts interaction, Mater. Werkst. 34 (2003) 1120–1128, https://doi.org/10.1002/mawe.200300699.

[4] G. Altankov, F. Grinnell, T. Groth, Studies on the biocompatibility of materials: fibroblast reorganization of substratum-bound fibronectin on surfaces varying in wettability, J. Biomed. Mater. Res. 30 (1996) 385–391, https://doi.org/10.1002/(SICI)1097-4636(199603)30:3<385::AID-JBM13>3.0.CO;2-J.

[5] M.S. Niepel, F. Almouhanna, B.K. Ekambaram, M. Menzel, A. Heilmann, T. Groth, Cross-linking multilayers of poly-l-lysine and hyaluronic acid: effect on mesenchymal stem cell behavior, Int. J. Artif. Organs 41 (2018) 223–235.

[6] N. Brizuela Guerra, C. González-García, V. Llopis, J. Carlos Rodríguez-Hernández, D. Moratal, P. Rico, M. Salmerón-Sánchez, Subtle variations in polymer chemistry modulate substrate stiffness and fibronectin activity, Soft Matter 6 (2010) 4748–4755, https://doi.org/10.1039/C0SM00074D.

[7] N. Faucheux, R. Schweiss, K. Lützow, C. Werner, T. Groth, Self-assembled monolayers with different terminating groups as model substrates for cell adhesion studies, Biomaterials 25 (2004) 2721–2730, https://doi.org/10.1016/j.biomaterials.2003.09.069.

[8] M. Tanaka, Design of novel 2D and 3D biointerfaces using self-organization to control cell behavior, Biochim. Biophys. Acta Gen. Subj. 1810 (2011) 251–258, https://doi.org/10.1016/j.bbagen.2010.10.002.

[9] N.J. Sniadecki, R.A. Desai, S.A. Ruiz, C.S. Chen, Nanotechnology for cell–substrate interactions, Ann. Biomed. Eng. 34 (2006) 59–74, https://doi.org/10.1007/s10439-005-9006-3.

[10] R.R. Costa, J.F. Mano, Polyelectrolyte multilayered assemblies in biomedical technologies, Chem. Soc. Rev. 43 (2014) 3453–3479, https://doi.org/10.1039/C3CS60393H.

[11] S.-H. Lee, H. Shin, Matrices and scaffolds for delivery of bioactive molecules in bone and cartilage tissue engineering, Adv. Drug Deliv. Rev. 59 (2007) 339–359, https://doi.org/10.1016/j.addr.2007.03.016.

[12] I. Antoniac (Ed.), Biologically Responsive Biomaterials for Tissue Engineering, Springer, New York, 2013.

[13] R.O. Hynes, Integrins: bidirectional, allosteric signaling machines, Cell 110 (2002) 673–687, https://doi.org/10.1016/S0092-8674(02)00971-6.

[14] S. Misra, V.C. Hascall, I. Atanelishvili, R. Moreno Rodriguez, R.R. Markwald, S. Ghatak, Utilization of glycosaminoglycans/proteoglycans as carriers for targeted therapy delivery, Int. J. Cell Biol. 2015 (2015) 25, 537560, https://doi.org/10.1155/2015/537560.

[15] I. Matsuo, C. Kimura-Yoshida, Extracellular distribution of diffusible growth factors controlled by heparan sulfate proteoglycans during mammalian embryogenesis, Phil. Trans. Biol. Sci. 369 (2014) 20130545, https://doi.org/10.1098/rstb.2013.0545.

[16] K.A. Davis, K.A. Burke, P.T. Mather, J.H. Henderson, Dynamic cell behavior on shape memory polymer substrates, Biomaterials 32 (2011) 2285–2293, https://doi.org/10.1016/j.biomaterials.2010.12.006.

[17] M. Zhao, G. Altankov, U. Grabiec, M. Bennett, M. Salmeron-Sanchez, F. Dehghani, T. Groth, Molecular composition of GAG-collagen I multilayers affects remodeling of terminal layers and osteogenic differentiation of adipose-derived stem cells, Acta Biomater. 41 (2016) 86–99, https://doi.org/10.1016/j.actbio.2016.05.023.

[18] J. Borges, J.F. Mano, Molecular interactions driving the layer-by-layer assembly of multilayers, Chem. Rev. 114 (2014) 8883–8942, https://doi.org/10.1021/cr400531v.

[19] R.F. Mhanna, J. Vörös, M. Zenobi-Wong, Layer-by-Layer films made from extracellular matrix macromolecules on silicone substrates, Biomacromolecules 12 (2011) 609–616, https://doi.org/10.1021/bm1012772.

[20] N. Monteiro, A. Martins, R.L. Reis, N.M. Neves, Liposomes in tissue engineering and regenerative medicine, J. R. Soc. Interface 11 (2014) 20140459, https://doi.org/10.1098/rsif.2014.0459.

[21] M. Çağdaş, A.D. Sezer, S. Bucak, Liposomes as Potential Drug Carrier Systems for Drug Delivery, Appl. Nanotechnol. Drug Deliv. (2014), https://doi.org/10.5772/58459.

[22] S. Pavlukhina, S. Sukhishvili, Polymer assemblies for controlled delivery of bioactive molecules from surfaces, Adv. Drug Deliv. Rev. 63 (2011) 822–836, https://doi.org/10.1016/j.addr.2011.03.017.

[23] M. Michel, D. Vautier, J.-C. Voegel, P. Schaaf, V. Ball, Layer by layer self-assembled polyelectrolyte multilayers with embedded phospholipid vesicles, Langmuir 20 (2004) 4835–4839, https://doi.org/10.1021/la049736q.

[24] D.V. Volodkin, P. Schaaf, H. Mohwald, J.-C. Voegel, V. Ball, Effective embedding of liposomes into polyelectrolyte multilayered films: the relative importance of lipid-polyelectrolyte and interpolyelectrolyte interactions, Soft Matter 5 (2009) 1394–1405, https://doi.org/10.1039/B815048F.

[25] T.G. Park, J.H. Jeong, S.W. Kim, Current status of polymeric gene delivery systems, Adv. Drug Deliv. Rev. 58 (2006) 467–486, https://doi.org/10.1016/j.addr.2006.03.007.

[26] P.P. Campos, L.F. Fraceto, M. Ferreira, Layer-by-layer films containing emodin or emodin encapsulated in liposomes for transdermal applications,, Colloids Surf. B Biointerfaces 162 (2018) 69–75, https://doi.org/10.1016/j.colsurfb.2017.11.030.

[27] S. Tassler, D. Pawlowska, C. Janich, J. Giselbrecht, S. Drescher, A. Langner, C. Wölk, G. Brezesinski, Lysine-based amino-functionalized lipids for gene transfection: 3D phase behaviour and transfection performance, Phys. Chem. Chem. Phys. 20 (2018) 17393–17405, https://doi.org/10.1039/C8CP01922C.

[28] C. Wölk, C. Janich, U. Bakowsky, A. Langner, G. Brezesinski, Malonic acid based cationic lipids - the way to highly efficient DNA-carriers, Adv. Colloid Interface Sci. 248 (2017) 20–34, https://doi.org/10.1016/j.cis.2017.08.003.

[29] X. Zhang, L. Dai, A. Wang, C. Wölk, B. Dobner, G. Brezesinski, Y. Tang, X. Wang, J. Li, The directional observation of highly dynamic membrane tubule formation induced by engulfed liposomes, Sci. Rep. 5 (2015) 16559, https://doi.org/10.1038/srep16559.

[30] M. Zhao, L. Li, C. Zhou, F. Heyroth, B. Fuhrmann, K. Maeder, T. Groth, Improved stability and cell response by intrinsic cross-linking of multilayers from collagen I and oxidized glycosaminoglycans, Biomacromolecules 15 (2014) 4272–4280, https://doi.org/10.1021/bm501286f.

[31] S. Tassler, C. Wölk, C. Janich, B. Dobner, G. Brezesinski, Lysine-based amino-functionalized lipids for gene transfection: the protonation state in monolayers at the air–liquid interface, Phys. Chem. Chem. Phys. 19 (2017) 20271–20280, https://doi.org/10.1039/C7CP03107F.

[32] U. Bhardwaj, D.J. Burgess, Physicochemical properties of extruded and non-extruded liposomes containing the hydrophobic drug dexamethasone, Int. J. Pharm. 388 (2010) 181–189, https://doi.org/10.1016/j.ijpharm.2010.01.003.

[33] J. Giselbrecht, C. Janich, S.R. Pinnapireddy, G. Hause, U. Bakowsky, C. Wölk, A. Langner, Overcoming the polycation dilemma - explorative studies to characterise the efficiency and biocompatibility of newly designed lipofection reagents, Int. J. Pharm. 541 (2018) 81–92, https://doi.org/10.1016/j.ijpharm.2018.02.029.

[34] F. Langenbach, J. Handschel, Effects of dexamethasone, ascorbic acid and β-glycerophosphate on the osteogenic differentiation of stem cells in vitro, Stem Cell Res. Ther. 4 (2013) 117, https://doi.org/10.1186/scrt328.

[35] P.R. Majhi, A. Blume, Temperature-induced micelle-vesicle transitions in DMPC−SDS and DMPC−DTAB mixtures studied by calorimetry and dynamic light scattering, J. Phys. Chem. B 106 (2002) 10753–10763, https://doi.org/10.1021/jp025849b.

[36] A. Zidovska, K.K. Ewert, J. Quispe, B. Carragher, C.S. Potter, C.R. Safinya, Block liposome and nanotube formation is a general phenomenon of two-component membranes containing multivalent lipids, Soft Matter 7 (2011) 8363–8369, https://doi.org/10.1039/C1SM05481C.

[37] K. Glinel, A. Moussa, A.M. Jonas, A. Laschewsky, Influence of polyelectrolyte charge density on the formation of multilayers of strong polyelectrolytes at low ionic strength, Langmuir 18 (2002) 1408–1412, https://doi.org/10.1021/la0113670.

[38] H. Al-Khoury, E. Espinosa-Cano, M.R. Aguilar, J.S. Román, F. Syrowatka, G. Schmidt, T. Groth, Anti-inflammatory surface coatings based on polyelectrolyte multilayers of heparin and polycationic nanoparticles of naproxen-bearing polymeric drugs, Biomacromolecules 20 (2019) 4015–4025, https://doi.org/10.1021/acs.biomac.9b01098.

[39] S.F. Himmelstoß, T. Hirsch, Long-term colloidal and chemical stability in aqueous media of NaYF4-type upconversion nanoparticles modified by ligand-exchange, Part. Part. Syst. Char. 36 (2019) 1900235, https://doi.org/10.1002/ppsc.201900235.

[40] R. Anouz, A. Repanas, E. Schwarz, T. Groth, Novel surface coatings using oxidized glycosaminoglycans as delivery systems of bone morphogenetic protein 2 (BMP-2) for bone regeneration, Macromol. Biosci. 18 (11) (2018), e1800283, https://doi.org/10.1002/mabi.201800283.

[41] O. Et-Thakafy, N. Delorme, C. Gaillard, et al., Mechanical properties of membranes composed of gel-phase or fluid-phase phospholipids probed on liposomes by atomic force spectroscopy, Langmuir 33 (21) (2017) 5117–5126, https://doi.org/10.1021/acs.langmuir.7b00363.

[42] P.C.F. da Câmara, R.C. Balaban, M. Hedayati, K.C. Popat, A.F. Martins, M.J. Kipper, Novel cationic tannin/glycosaminoglycan-based polyelectrolyte multilayers promote stem cells adhesion and proliferation, RSC Adv. 9 (2019) 25836–25846, https://doi.org/10.1039/C9RA03903A.

[43] J.H. Lee, H.B. Lee, A wettability gradient as a tool to study protein adsorption and cell adhesion on polymer surfaces, J. Biomater. Sci. Polym. Ed. 4 (1993) 467–481, https://doi.org/10.1163/156856293x00131.

[44] S. Mochizuki, N. Kanegae, K. Nishina, Y. Kamikawa, K. Koiwai, H. Masunaga, K. Sakurai, The role of the helper lipid dioleoylphosphatidylethanolamine (DOPE) for DNA transfection cooperating with a cationic lipid bearing ethylenediamine, Biochim. Biophys. Acta Biomembr. 1828 (2013) 412–418, https://doi.org/10.1016/j.bbamem.2012.10.017.

[45] G. Sondag, S. Salihoglu, S. Lababidi, D. Crowder, F. Moussa, S. Abdelmagid, F. Safadi, Osteoactivin induces transdifferentiation of C2C12 myoblasts into osteoblasts, J. Cell. Physiol. 229 (2014), https://doi.org/10.1002/jcp.24512.

[46] M.J. Dalby, A.J. García, M. Salmeron-Sanchez, Receptor control in mesenchymal stem cell engineering, Nature Rev. Mater. 3 (2018) 1–14, https://doi.org/10.1038/natrevmats.2017.91.

[47] M. Mullaney, T. Groth, R. Darkow, R. Hesse, W. Albrecht, D. Paul, G. von Sengbusch, Investigation of plasma protein adsorption on functionalized nanoparticles for application in apheresis, Artif. Organs 23 (1999) 87–97, https://doi.org/10.1046/j.1525-1594.1999.06280.x.

[48] N. Davidenko, C.F. Schuster, D.V. Bax, R.W. Farndale, S. Hamaia, S.M. Best, R.E. Cameron, Evaluation of cell binding to collagen and gelatin: a study of the effect of 2D and 3D architecture and surface chemistry, J. Mater. Sci. Mater. Med. 27 (2016) 148, https://doi.org/10.1007/s10856-016-5763-9.

[49] D. Needham, J.-Y. Park, A.M. Wright, J. Tong, Materials characterization of the low temperature sensitive liposome (LTSL): effects of the lipid composition (lysolipid

and DSPE–PEG2000) on the thermal transition and release of doxorubicin, Faraday Discuss 161 (2013) 515–534, https://doi.org/10.1039/C2FD20111A.

[50] N. Monteiro, A. Martins, D. Ribeiro, S. Faria, N.A. Fonseca, J.N. Moreira, R.L. Reis, N.M. Neves, On the use of dexamethasone-loaded liposomes to induce the osteogenic differentiation of human mesenchymal stem cells, J. Tissue Eng. Regen. Med. 9 (2015) 1056–1066, https://doi.org/10.1002/term.1817.

[51] N. Tran, X. Mulet, A.M. Hawley, T.M. Hinton, S.T. Mudie, B.W. Muir, E.C. Giakoumatos, L.J. Waddington, N.M. Kirby, C.J. Drummond, Nanostructure and cytotoxicity of self-assembled monoolein–capric acid lyotropic liquid crystalline nanoparticles, RSC Adv. 5 (2015) 26785–26795, https://doi.org/10.1039/C5RA02604K.